Communication in a Poisson Field of Interferers

by

Pedro C. Pinto

Licenciatura, Electrical and Computer Engineering
Oporto University (2003)

Submitted to the Department of Electrical Engineering and Computer Science
in partial fulfillment of the requirements for the degree of
Master of Science in Electrical Engineering

at the

MASSACHUSETTS INSTITUTE OF TECHNOLOGY
{February 2007}
September 2006

Author .....
Department of Electrical Engineering and Computer Science
September 11, 2006

Certified by .....
Moe Z. Win
Associate Professor
Thesis Supervisor

Accepted by .....
Arthur C. Smith
Chairman, Department Committee on Graduate Students

Communication in a Poisson Field of Interferers

by

Pedro C. Pinto

Submitted to the Department of Electrical Engineering and Computer Science
on September 11, 2006, in partial fulfillment of the requirements for the degree of
Master of Science in Electrical Engineering

Abstract

This thesis presents a mathematical model for communication subject to both interference and noise. We introduce a realistic framework where the interferers are spatially scattered according to a Poisson field, and are operating asynchronously in a wireless environment subject to path loss, shadowing, and multipath fading. We consider both cases of slow and fast-varying interferer positions. Under this scenario, we determine the statistical distribution of the cumulative interference at the output of a linear receiver, located anywhere in the two-dimensional plane. We characterize the error probability and capacity of the link, when subject to both network interference and thermal noise. We derive the power spectral density (PSD) of the cumulative interference at any location in the plane. We put forth the concept of spectral outage probability (SOP), a new characterization of the cumulative interference generated by communicating nodes in a wireless network. Lastly, we quantify the cumulative interference distribution, error probability, channel capacity, PSD, and SOP as a function of various important system parameters, such as the signal-to-noise ratio (SNR), interference-to-noise ratio (INR), path loss exponent of the channel, and spatial density of the interferers.
The proposed model is valid for any linear modulation scheme (e.g., M-ary phase shift keying or M-ary quadrature amplitude modulation), and captures all the essential physical parameters that affect network interference. Nevertheless, it is simple enough to enable a tractable analysis and provide fundamental insights that may be of value to the network designer. Finally, this work generalizes the conventional analysis of linear detection in the presence of additive white Gaussian noise (AWGN) and fast fading, allowing the traditional results to be extended to include the effect of interference.

Thesis Supervisor: Moe Z. Win
Title: Associate Professor

Acknowledgments

Many individuals have contributed to the success of this thesis. I am deeply grateful to my advisor, Professor Moe Win, whose genuine support, enthusiasm, and advice have been invaluable over the past two years, in both professional and personal terms. Not only has he provided guidance through the intricacies of research, but he has also helped in broadening my mind as a scientist and an individual.

I am indebted to Professor Alan Oppenheim for his counsel and mentoring since my arrival to MIT. His advice has enabled me to better understand life and work at MIT, and easily overcome all the difficulties that incoming students face.

I am thankful to Professor Marco Chiani and Professor Andrea Giorgetti at the University of Bologna, for invaluable discussions on relevant metrics for characterization of wireless systems; careful reading of the thesis manuscript; and advice on the extension of the results to ultrawideband communications.

I thank L. A. Shepp, L. Greenstein, J. H. Winters, and G. J. Foschini, for insightful comments regarding Poisson fields, outage metrics, spectral coexistence, and multi-antenna systems.

I also thank my colleagues in the Wireless Communications Group at LIDS, for their wise advice about the inner workings of MIT and LIDS, over the past two years.

Most importantly, I am greatly indebted to my family, for their unwavering encouragement to pursue my interests, and limitless support in all facets of life.

This research was supported, in part, by the Portuguese Science and Technology Foundation under grant SFRH-BD-17388-2004, the Charles Stark Draper Laboratory Robust Distributed Sensor Networks Program, the Office of Naval Research Young Investigator Award N00014-03-1-0489, and the National Science Foundation under Grant ANI-0335256.

Contents

List of Figures

List of Tables

Abbreviations

AWGN	additive white Gaussian noise
c.d.f.	cumulative distribution function
CS	circularly symmetric
FCC	Federal Communications Commission
GPS	Global Positioning System
i.i.d.	independent identically distributed
INR	interference-to-noise ratio
IQ	in-phase/quadrature
M-PAM	M-ary pulse amplitude modulation
M-QAM	M-ary quadrature amplitude modulation
p.d.f.	probability density function
PSD	power spectral density
r.v.	random variable
SNR	signal-to-noise ratio
SOP	spectral outage probability
WSS	wide-sense stationary

WSCS wide-sense cyclostationary

Notation

$\mathbb{P}\{\mathcal{A}\}$	probability of event $\mathcal{A}$; also $\mathbb{P}_{\mathcal{A}}\{\mathcal{A}\}$
$\mathbb{E}\{X\}$	expected value of random variable X; also $\mathbb{E}_X\{X\}$ and $\overline{X}$
$\mathbb{E}\|X\|^a$	$\mathbb{E}\{\|X\|^a\}$
$\mathbb{V}\{X\}$	variance of random variable X
$I(X;Y)$	mutual information between random variables X and Y
$X \sim$	the distribution of the real random variable X
$\mathbf{X} \sim$	the distribution of the complex random variable $\mathbf{X}$
$X \overset{\|Y}{\sim}$	the distribution of random variable X conditional on Y
$\mathcal{U}(a,b)$	uniform distribution in the interval $[a,b]$
$\mathcal{E}xp(\lambda)$	exponential distribution with mean $1/\lambda$
$\mathcal{N}(\mu,\sigma^2)$	real Gaussian distribution with mean μ and variance σ^2
$\mathcal{N}_c(0,\sigma^2)$	circularly symmetric complex Gaussian distribution, where the real and imaginary parts are independent, identically distributed $\mathcal{N}(0,\sigma^2/2)$
$\mathcal{S}(\alpha,\beta,\gamma)$	real stable distribution with characteristic exponent α, skewness β, dispersion γ, and location $\mu = 0$
$\mathcal{S}_c(\alpha,\beta,\gamma)$	circularly symmetric complex stable distribution, where the real and imaginary parts are independent, identically distributed $\mathcal{S}(\alpha,\beta,\gamma)$

$f_X(x)$	probability density function of random variable X
$F_X(x)$	cumulative distribution function of random variable X
$\exp(x)$	e^x
$\log_2(x)$	base 2 logarithm
$\ln(x)$	natural logarithm
$\text{sign}(x)$	signum function
$Q(x)$	Gaussian Q function; $Q(x) = \frac{1}{\sqrt{2\pi}} \int_x^\infty e^{-\frac{t^2}{2}} dt$
$\Gamma(x)$	Gamma function; $\Gamma(x) = \int_0^\infty t^{x-1} e^{-t} dt$
$\text{Ei}(x)$	Exponential integral function; $\text{Ei}(x) = -\int_{-x}^\infty \frac{e^{-t}}{t} dt$
$u(x)$	unit-step function
$\|x(t)\|$	$\mathcal{L}_2$ norm of $x(t)$; $\|x(t)\| = \sqrt{\int_{-\infty}^{+\infty} \|x(t)\|^2 dt}$
$\mathcal{F}\{x(t)\}$	Fourier transform of $x(t)$
$\mathbb{R}$	real numbers
$\mathbb{C}$	complex numbers
j	imaginary unit
$\mathbf{x}^*$	complex conjugate of $\mathbf{x}$
$\text{Re}\{\mathbf{x}\}$	real part of $\mathbf{x}$
$\text{Im}\{\mathbf{x}\}$	imaginary part of $\mathbf{x}$
$\mathbf{I}$	identity matrix

Chapter 1

Introduction

1.1 Interference Modeling

In a wireless network composed of many spatially scattered nodes, there are two fundamental impairments that constrain the communication between nodes: *thermal noise* and *network self-interference*. Thermal noise is introduced by the receiver electronics and is usually modeled as AWGN, which constitutes a good approximation in most cases. Self-interference, on the other hand, is due to other transmitter nodes, whose radiated signals affect receiver nodes of the same network. For simplicity, interference is typically approximated by AWGN with some given power [1, 2]. However, this elementary model does not capture the physical parameters that affect self-interference, namely: 1) the spatial distribution of nodes in the network; 2) the transmission characteristics of nodes, such as modulation, power, and synchronization; and 3) the propagation characteristics of the medium, such as path loss, shadowing, and multipath fading. If, instead, we use a Poisson point process to model the user positions, then all these parameters are easily accounted for, and appear explicitly in the resulting performance expressions.

The application of the Poisson field model to cellular networks was first investigated in [3] and later advanced in [4]. However, the authors either ignore random propagation effects (such as shadowing and multipath fading), or restrict the analysis to error

probability in non-coherent FSK modulations. In other related work [5], it is assumed that the different interferers are synchronized at the symbol or slot level, which is typically unrealistic. In [6,7], the authors choose a different approach and restrict the node locations to a disk or ring in the two-dimensional plane. Although this ensures the number of interferers is finite, it complicates the analysis and does not provide useful insights into the interference problem. Lastly, none of the mentioned studies attempts a spectral characterization of the interference, focusing instead on other performance metrics.

1.2 Thesis Objectives and Organization

The main research contributions of this thesis are as follows:

- We introduce a realistic framework where the interferers are spatially scattered according to an infinite Poisson field, and are operating asynchronously in a wireless environment subject to path loss, log-normal shadowing, and fast fading. Our analysis is valid for any linear modulation scheme, and easily accounts for all the essential physical parameters that affect network interference, which appear explicitly in the resulting performance expressions.

- We specifically address two different scenarios: one where the interfering nodes are slow-moving, and another where they are fast-moving.

- We determine the statistical distribution of the cumulative interference at the output of a linear receiver, located anywhere in the two-dimensional plane.

- We characterize the error performance of the link (in terms of average and outage probabilities) when subject to both interference and thermal noise, for any linear modulation scheme.

- We analyze and provide expressions for the capacity of the link, when subject to both network self-interference and thermal noise.

- We derive the power spectral density (PSD) of the cumulative interference at any location in the two-dimensional plane, for any linear modulation scheme.

- We put forth the concept of spectral outage probability (SOP), a new characterization of the cumulative interference generated by communicating nodes in a wireless network.

- We quantify the cumulative interference distribution, error performance, channel capacity, PSD, and SOP as a function of various important system parameters, such as the signal-to-noise ratio (SNR), interference-to-noise ratio (INR), path loss exponent, and spatial density of the interferers. Our analysis clearly shows how the system performance depends on these parameters, thereby providing insights that may be of value to the network designer.

The thesis is organized as follows. Chapter 1 presents the scope and contributions of the thesis, and briefly reviews stable distributions. Chapter 2 describes the system model. Chapter 3 derives the baseband representation and distribution of the cumulative interference. Chapter 4 analyzes the error performance of the system. Chapter 5 analyzes the channel capacity. Chapter 6 characterizes the spectrum of the cumulative interference and introduces the concept of spectral outage probability. Chapter 7 concludes the thesis and suggests directions for future research.

1.3 Review of Stable Distributions

In the framework proposed in this thesis, stable distributions play an important role in the modelling of interference. Stable laws are a direct generalization of Gaussian distributions, and include other densities with heavier (algebraic) tails. They share many properties with Gaussian distributions, namely the stability property and the generalized central limit theorem [8, 9].

A r.v. X is defined to be *stable distributed* if its characteristic function $\phi_X(\omega) =$

$\mathbb{E}\{e^{j\omega X}\}$ has the form [8]

$$\phi_X(\omega) = \begin{cases} \exp\left[-\gamma|\omega|^\alpha\left(1 - j\beta\,\text{sign}(\omega)\tan\frac{\pi\alpha}{2}\right) + j\omega\mu\right], & \alpha \neq 1, \\ \exp\left[-\gamma|\omega|\left(1 + j\frac{2}{\pi}\beta\,\text{sign}(\omega)\ln|\omega|\right) + j\omega\mu\right], & \alpha = 1. \end{cases}$$

A real stable distribution can therefore be characterized by four parameters:

$\alpha \in (0, 2]$ Characteristic exponent, which controls the heaviness of the p.d.f. tail. If $\alpha = 2$, then $X \sim \mathcal{N}(\mu, 2\gamma)$.

$\beta \in [-1, 1]$ Skewness parameter. The cases where $\beta < 0$, $\beta = 0$, $\beta > 0$ correspond to a p.d.f. which is skewed to the left, symmetric around the center μ, and skewed to the right, respectively.

$\gamma \in [0, \infty)$ Dispersion parameter, which behaves like the variance.

$\mu \in \mathbb{R}$ Location parameter, which behaves like the mean.

We use $X \sim \mathcal{S}(\alpha, \beta, \gamma, \mu)$ to denote that r.v. X has a real stable distribution with parameters α, β, γ, and μ.[1] When $\beta = \mu = 0$, the r.v. X is said to be *symmetric stable*. Figures 1.1 to 1.3 depict stable p.d.f.'s for various parameters α, β, and γ.

Some useful properties of stable r.v.'s which are used in this thesis are provided below.

Property 1.1 (Scaling Property). *Let $X \sim \mathcal{S}(\alpha, \beta, \gamma)$ with $\alpha \neq 1$, and let k be a non-zero real constant. Then,*

$$kX \sim \mathcal{S}(\alpha,\ \text{sign}(k)\beta,\ |k|^\alpha\gamma).$$

Property 1.2 (Decomposition Property). *Let $X \sim \mathcal{S}(\alpha, 0, \gamma)$. Then, X can be decomposed as*

$$X = \sqrt{V}G,$$

[1] Unless otherwise indicated, in this thesis we only deal with distributions where $\mu = 0$, and therefore use the simplified notation $X \sim \mathcal{S}(\alpha, \beta, \gamma)$.

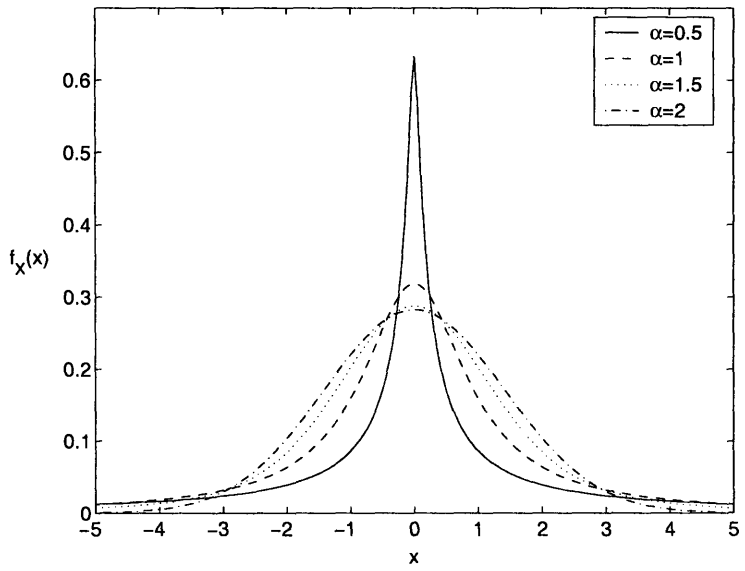

(a) Center part of the PDFs.

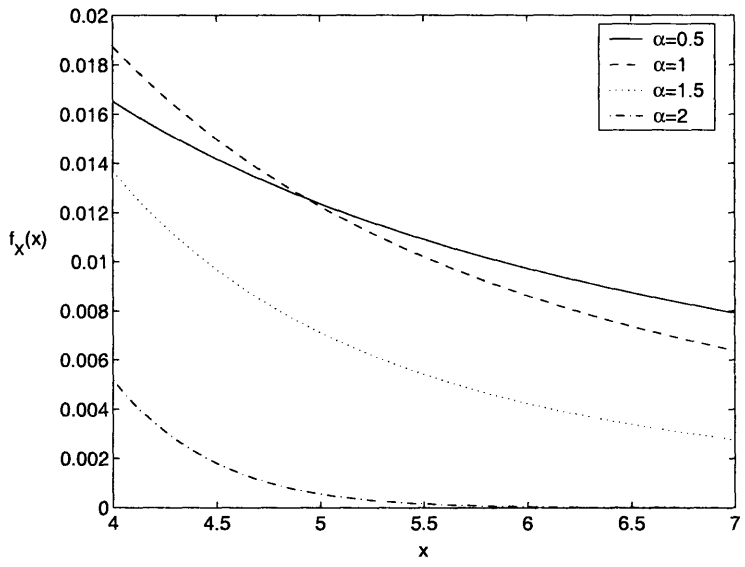

(b) Tail of the PDFs.

Figure 1.1: Stable densities for varying characteristic exponents α ($\beta = 0$, $\gamma = 1$, $\mu = 0$).

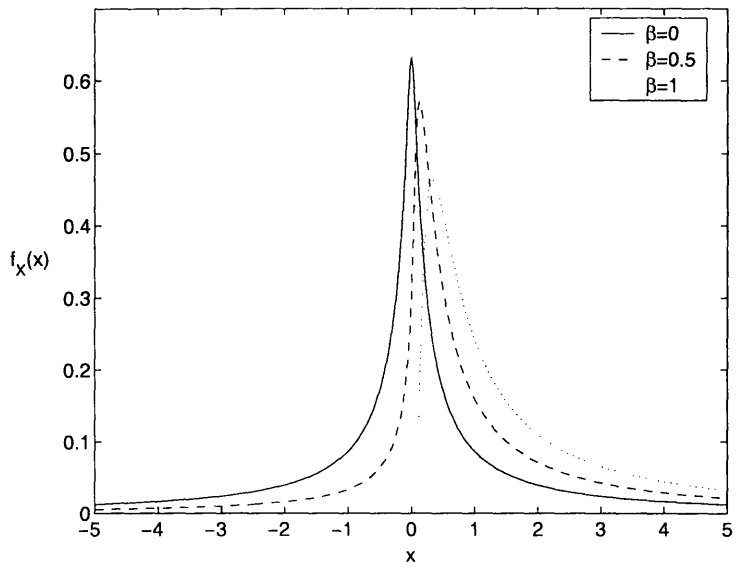

Figure 1.2: Stable densities for varying skewness parameters β ($\alpha = 0.5$, $\gamma = 1$, $\mu = 0$).

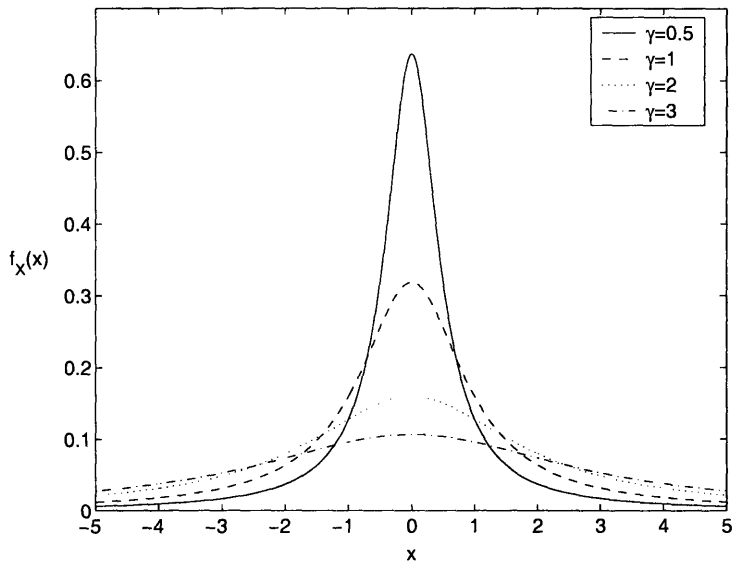

Figure 1.3: Stable densities for varying dispersion parameters γ ($\alpha = 1$, $\beta = 0$, $\mu = 0$).

where $V \sim \mathcal{S}\left(\frac{\alpha}{2}, 1, \cos\frac{\pi\alpha}{4}\right)$ *and* $G \sim \mathcal{N}(0, 2\gamma^{2/\alpha})$. *In addition,* V *and* G *are independent r.v.'s.*

A more detailed treatment of stables distributions, including its definitions and properties, can be found in [8–11].

Chapter 2

System Model

2.1 Spatial Distribution of the Nodes

In the proposed model, we account for the spatial distribution of users by assuming an infinite number of nodes distributed according to a homogeneous Poisson point process in the two-dimensional plane. Typically, the terminal positions are unknown to the network designer a priori, so we may as well treat them as completely random and use a Poisson point process.

A two-dimensional homogeneous Poisson point process is characterized by the following properties [12]:

1. If $N(\mathcal{R})$ denotes the number of nodes located inside a region $\mathcal{R}$ of the plane, then the r.v.'s $N(\mathcal{R}_i)$ are independent if the regions $\mathcal{R}_i$ are non-overlapping.

2. Given that a node is inside region $\mathcal{R}$, its position is uniformly distributed in that region.

3. The probability $\mathbb{P}\{k \text{ in } \mathcal{R}\}$ of k nodes being inside region $\mathcal{R}$ depends only on the area $A_{\mathcal{R}}$ of the region (not on its shape or location in the plane), and follows a Poisson distribution given by

$$\mathbb{P}\{k \text{ in } \mathcal{R}\} = \frac{(\lambda A_{\mathcal{R}})^k}{k!} e^{-\lambda A_{\mathcal{R}}}, \quad k \geq 0,$$

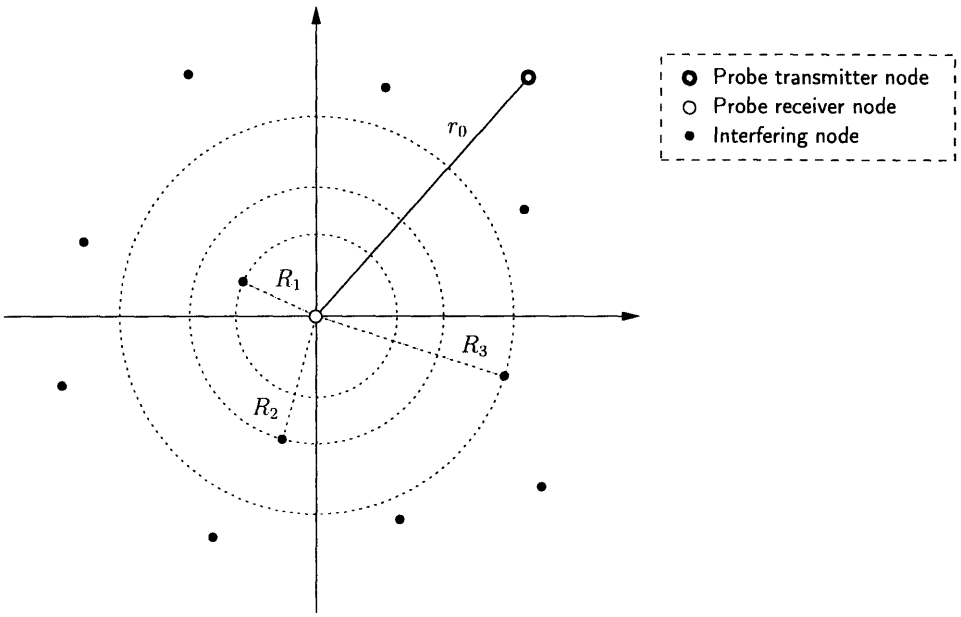

Figure 2.1: Poisson field model for the spatial distribution of nodes.

where λ is the (constant) spatial density of nodes, in nodes per unit area.

The Poisson point process can then be described by the single parameter λ, which we use to denote the spatial density of *interfering nodes*. We define the interfering nodes to be all terminals which are transmitting within the frequency band of interest, during the time interval of interest (e.g., a symbol or packet time), and hence are effectively contributing to the interference. Then, irrespective of the network topology (e.g., point-to-point or broadcast) or multiple-access technique (e.g., time or frequency hopping), the proposed model depends only on the density λ of interfering nodes.[1] In what follows, we will use interchangeably the terms *node*, *interferer*, *user* and *terminal* to mean *interfering node*.

The proposed spatial model is depicted in Fig. 2.1. For analytical purposes, we assume there is a *probe link* composed of two *probe nodes*: one receiver node, located at the origin, and one transmitter node (node $i = 0$), deterministically located at a distance r_0 from the origin.[2] All the other nodes ($i = 1 \ldots \infty$) are interfering nodes,

[1]Time and frequency hopping can be easily accommodated in this model, using the splitting property of Poisson processes to obtain the *effective* density of nodes that contribute to the interference.

[2]Lowercase letters are used to denote *deterministic* quantities, while uppercase letters are used for

whose random distances to the origin are denoted by $\{R_i\}_{i=1}^{\infty}$, where $R_1 \leq R_2 \leq \ldots$. Our goal is then to determine the effect of the interfering nodes on the probe link.

2.2 Transmission Characteristics of the Nodes

To account for the transmission characteristics of users, we consider that all interfering nodes employ the same linear modulation scheme, such as M-ary phase shift keying (M-PSK) or M-ary quadrature amplitude modulation (M-QAM). Furthermore, they all transmit at the same power P – a plausible constraint when power control is too complex to implement (e.g., decentralized ad-hoc networks). For generality, however, we allow the probe transmitter to employ an arbitrary linear modulation and arbitrary power P_0, not necessarily equal to those used by the interfering nodes.

The case where the probe and interfering nodes use a *different* modulation and power may correspond to an heterogeneous scenario with a large number of identical secondary users (e.g., cognitive-radio terminals) interfering on a primary link. The case where the probe and interfering nodes use the *same* modulation and power, on the other hand, may correspond to a sensor network scenario, where there is a large number of indistinguishable, spatially scattered nodes, with similar transmission characteristics.

In terms of synchronization, we consider an asynchronous system where different terminals are allowed to operate independently. As depicted in Fig. 2.2, node i transmits with a random delay D_i relative to node 0, where $D_i \sim \mathcal{U}(0,T)$. Thus, node 0 initiates symbol transmissions at times nT by convention, while node i initiates symbol transmissions at times $nT + D_i$. Note that to analyze the error probability and channel capacity, we only need to consider one symbol interval, $0 \leq t \leq T$; to characterize the spectrum of interference, on the other hand, we need consider the waveforms over all time, $-\infty < t < +\infty$.

Lastly, in terms of demodulation, the probe receiver[3] employs a conventional linear detector. Typically, parameters such as the spatial density of interferers and the prop-

stochastic quantities.

[3]The other receiver nodes are not relevant for the analysis, since they do not cause interference.

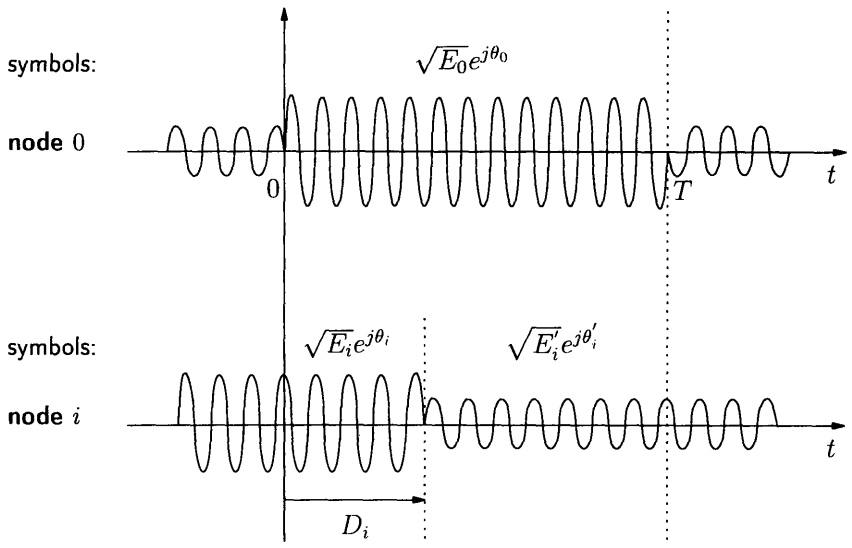

Figure 2.2: Asynchronism between different transmitting nodes. In the observation interval $[0, T]$, a change in constellation symbol of node i occurs at random time $t = D_i$, from $\sqrt{E_i}e^{j\theta_i}$ to $\sqrt{E_i'}e^{j\theta_i'}$. The distribution of D_i is assumed to be $\mathcal{U}(0, T)$.

agation characteristics of the medium (e.g., shadowing and path loss parameters) are unknown to the receiver. This lack of information about the interference, together with constraints on receiver complexity, justify the use of a simple linear detector, which is optimal in the presence of AWGN.

2.3 Propagation Characteristics of the Medium

To account for the propagation characteristics of the environment, we assume a $1/r^b$ median signal amplitude decay with distance r. The parameter b is environment-dependent, and can approximately range from 1 (e.g., hallways inside buildings) to 4 (e.g., dense urban environments).[4] Table 2.1 gives typical values of b for different environments [13, 14]. The use of such decay law also ensures that interferers located far away from the origin have a negligible contribution to the total interference observed at that point, thus making the infinite-plane assumption reasonable.

[4]In this thesis, we will refer to b as the "amplitude loss exponent", which corresponds to a decay in *signal amplitude*, not in *signal power*.

Environment	Range for b
Free space	1
Two-ray model	2
Urban macrocell	$1.8 - 3.5$
Urban microcell	$1.3 - 1.7$
Office building	$1 - 3$
Factory	$0.8 - 1.6$
Home	1.5

Table 2.1: Typical signal amplitude loss exponents b for various environments.

Experimental results show that the $1/r^b$ deterministic propagation law is only the median behavior of the signal. Typically, a signal transmitted through a wireless channel will experience random variation due to blockage from objects in the signal path (shadowing), and constructive-destructive addition of different multipath components (multipath fading). These two random effects are independent and multiplicative.

In this thesis, we use a log-normal model to capture the shadowing effect. Specifically, the corresponding received signal strength S is log-normal distributed with p.d.f. given by

$$f_S(s) = \frac{1}{s\sigma\sqrt{2\pi}} \exp\left[-\frac{1}{2\sigma^2} \ln^2\left(\frac{s}{\mu}\right)\right], \quad s \geq 0, \tag{2.1}$$

where $\mu = K/r^b$ is the median of S for some constant K, and $\sigma = \sigma_s/2$. The parameter σ_s is the standard deviation of the instantaneous power, whose typical values range from 6 to 12 dB, depending on the environment [15, 16]. In this model, the shadowing is responsible for random fluctuations in the signal level around the deterministic path loss K/r^b. A useful fact is that a log-normal r.v. S with parameters μ and σ can be expressed as $S = \mu e^{\sigma G}$, where $G \sim \mathcal{N}(0, 1)$.

The multipath effect is modeled as frequency-flat Rayleigh fading, which is superimposed on the path-loss and shadowing of (2.1). Specifically, the Rayleigh fading affects the received signal by introducing a random phase $\phi \sim \mathcal{U}(0, 2\pi)$, as well as an amplitude

factor α which is Rayleigh distributed with p.d.f. given by

$$f_\alpha(a) = \frac{a}{\widetilde{\sigma}^2} \exp\left(-\frac{a^2}{2\widetilde{\sigma}^2}\right), \quad a \geq 0. \tag{2.2}$$

For normalization purposes, the parameter $\widetilde{\sigma}$ is chosen such that the fading has unit power gain, i.e., $\mathbb{E}\{\alpha^2\} = 1$.

We have thus a combined model for the path-loss, log-normal shadowing, and Rayleigh fading, where the overall effect of the channel propagation is captured by an amplitude factor $\frac{\alpha e^{\sigma G} K}{r^b}$ and a uniform phase ϕ. The variations in the signal level due to shadowing are usually slow, since they occur over distances that are proportional to the length of the obstruction object (typically, $10 - 100$ m). On the other hand, the variations due to multipath fading are usually fast, occurring over distances on the order of the signal wavelength.

In the following chapters, we assume the shadowing and multipath fading are independent for different nodes i, and approximately constant during at least one symbol interval. Additionally, the probe receiver can perfectly estimate the shadowing and fading affecting its own link, hence ensuring that coherent demodulation of the desired signal is possible.

Chapter 3

Representation and Distribution of the Interference

In this chapter, we characterize the cumulative interference measured at the origin of the two-dimensional plane, in terms of its probability distribution. Two distinct scenarios are considered: one where the interfering nodes are immobile or slow-moving, and the other where their positions change quickly with time. The resulting probability distributions will be used in later chapters to analyze the error probability and capacity of the probe link.

3.1 Complex Baseband Representation of the Interference

Under the system model described in Chapter 2, the cumulative signal $Z(t)$ received by the probe node at the origin can be written as

$$Z(t) = \frac{\alpha_0 e^{\sigma G_0}}{r_0^b}\sqrt{\frac{2E_0}{T}}\cos(2\pi f_c t + \theta_0) + Y(t) + W(t), \quad 0 \leq t \leq T, \tag{3.1}$$

where the first right-hand term is the desired signal from the transmitter probe node, $Y(t)$ is the cumulative interference with

$$Y(t) = \sum_{i=1}^{\infty} \left(\frac{\alpha_i e^{\sigma G_i}}{R_i^b} \sqrt{\frac{2E_i}{T}} \cos(2\pi f_c t + \theta_i + \phi_i) u(D_i - t) \right.$$
$$\left. + \frac{\alpha_i e^{\sigma G_i}}{R_i^b} \sqrt{\frac{2E_i'}{T}} \cos(2\pi f_c t + \theta_i' + \phi_i) u(t - D_i) \right), \quad 0 \le t \le T, \quad (3.2)$$

and $W(t)$ is the AWGN with two-sided power spectral density $N_0/2$, and independent of $Y(t)$.

The overall effect of the path loss, log-normal shadowing, and Rayleigh fading on node i is captured by the amplitude factor $\alpha_i e^{\sigma G_i}/R_i^b$, where $G_i \sim \mathcal{N}(0,1)$, and by the uniform phase ϕ_i.[1] The meaning of the remaining parameters is apparent from Fig. 2.2. We assume that r.v.'s α_i, ϕ_i, G_i, D_i, E_i, E_i', θ_i, and θ_i' are statistically independent for different nodes i. In addition, each node transmits a sequence of i.i.d. symbols.

The probe node located at the origin receives and demodulates the cumulative signal $Z(t)$, using a simple linear detector. This can be achieved by projecting $Z(t)$ onto the orthonormal set $\{\psi_1(t) = \sqrt{\frac{2}{T}} \cos(2\pi f_c t), \psi_2(t) = -\sqrt{\frac{2}{T}} \sin(2\pi f_c t)\}$. By defining $Z_j = \int_0^T Z(t)\psi_j(t)dt$, $j = 1, 2$, we can write

$$Z_1 = \frac{\alpha_0 e^{\sigma G_0}}{r_0^b} \sqrt{E_0} \cos\theta_0 + Y_1 + W_1 \quad (3.3)$$

$$Z_2 = \frac{\alpha_0 e^{\sigma G_0}}{r_0^b} \sqrt{E_0} \sin\theta_0 + Y_2 + W_2, \quad (3.4)$$

where W_1 and W_2 are $\mathcal{N}(0, N_0/2)$ and mutually independent. After some algebra (Appendix A), Y_1 and Y_2 can be expressed as

$$Y_1 = \int_0^T Y(t)\psi_1(t)dt = \sum_{i=1}^{\infty} \frac{e^{\sigma G_i} X_{i1}}{R_i^b} \quad (3.5)$$

$$Y_2 = \int_0^T Y(t)\psi_2(t)dt = \sum_{i=1}^{\infty} \frac{e^{\sigma G_i} X_{i2}}{R_i^b}, \quad (3.6)$$

[1]Since we assume the probe receiver perfectly estimates the phase ϕ_0 of the multipath fading affecting its own link, we can set $\phi_0 = 0$ without loss of generality.

where

$$X_{i1}= \alpha_i \left[\sqrt{E_i}\frac{D_i}{T}\cos(\theta_i+\phi_i) + \sqrt{E_i'}\left(1-\frac{D_i}{T}\right)\cos(\theta_i'+\phi_i)\right] \tag{3.7}$$

$$X_{i2}= \alpha_i \left[\sqrt{E_i}\frac{D_i}{T}\sin(\theta_i+\phi_i) + \sqrt{E_i'}\left(1-\frac{D_i}{T}\right)\sin(\theta_i'+\phi_i)\right]. \tag{3.8}$$

By defining the following complex quantities[2]

$$\mathbf{Z} = Z_1 + jZ_2$$

$$\mathbf{Y} = Y_1 + jY_2$$

$$\mathbf{W} = W_1 + jW_2$$

$$\mathbf{X}_i = X_{i1} + jX_{i2},$$

we can rewrite (3.3)-(3.8) in complex baseband notation as

$$\mathbf{Z} = \frac{\alpha_0 e^{\sigma G_0}}{r_0^b}\sqrt{E_0}e^{j\theta_0} + \mathbf{Y} + \mathbf{W} \tag{3.9}$$

$$\mathbf{Y} = \sum_{i=1}^{\infty}\frac{e^{\sigma G_i}\mathbf{X}_i}{R_i^b} \tag{3.10}$$

where

$$\mathbf{X}_i = \alpha_i e^{j\phi_i}\left[\frac{D_i}{T}\sqrt{E_i}e^{j\theta_i} + \left(1-\frac{D_i}{T}\right)\sqrt{E_i'}e^{j\theta_i'}\right], \tag{3.11}$$

and the distribution of $\mathbf{W}$ is given by

$$\mathbf{W} \sim \mathcal{N}_c(0, N_0). \tag{3.12}$$

Since different interferers i transmit asynchronously and independently, the r.v.'s $\{\mathbf{X}_i\}_{i=1}^{\infty}$ are also independent.

In what follows, we derive the distribution of $\mathbf{Y}$ for two important cases: the $\mathcal{P}$-conditioned and unconditional cases. We will use $\mathcal{P}$ as a shorthand for *"a particular realization of the location* $\{R_i\}_{i=1}^{\infty}$ *and shadowing* $\{G_i\}_{i=1}^{\infty}$ *of the interferers"*, or

[2]Boldface letters are used to denote complex quantities.

more succinctly, the *"position of the interferers"*. The $\mathcal{P}$-conditioned characterization of $\mathbf{Y}$ is useful in scenarios where the interfering nodes are immobile or slow-moving. The unconditional characterization, on the other hand, is relevant when the interferer positions change quickly in time.

3.2 $\mathcal{P}$-conditioned Interference Distribution

Consider, for example, a congested urban scenario where the interfering nodes are spatially scattered. These nodes are subject to shadowing due to blockage from the surrounding buildings and trees. Typically, the movement of the nodes during the interval of interest (e.g., a symbol or packet time) is negligible. This has two implications: 1) the distances $\{R_i\}_{i=1}^{\infty}$ of the interferers to the origin vary slowly; and 2) the shadowing $\{G_i\}_{i=1}^{\infty}$ affecting those nodes also varies slowly, since the shadowing is itself associated with the movement of the nodes near large blocking objects. In this *quasi-static* scenario, it is insightful to condition the interference analysis on a given realization $\mathcal{P}$ of the distances $\{R_i\}_{i=1}^{\infty}$ and shadowing $\{G_i\}_{i=1}^{\infty}$ of the interferers. This will enable the derivation of the error outage probability of the probe link – a more meaningful metric than the average error probability, in the case of slow-varying $\mathcal{P}$ [17]. Because of its fast nature, the Rayleigh fading is averaged out in the analysis, no matter whether we condition on $\mathcal{P}$ or not.

We now derive the $\mathcal{P}$-conditioned distribution of the cumulative interference $\mathbf{Y}$ given in (3.10)-(3.11). The work in [18] shows that $\mathbf{X}_i$ in (3.11) can be well approximated by a CS complex Gaussian r.v., such that

$$\mathbf{X}_i \sim \mathcal{N}_c(0, 2V_X), \quad V_X = \mathbb{V}\{X_{ij}\}, \quad i \geq 1. \tag{3.13}$$

Then, conditioned on $\mathcal{P}$, the interference $\mathbf{Y} = \sum_{i=1}^{\infty} \frac{e^{\sigma G_i}\mathbf{X}_i}{R_i^b}$ becomes a sum of independent CS Gaussian r.v.'s and is therefore a CS Gaussian r.v. given by

$$\mathbf{Y} \overset{|\mathcal{P}}{\sim} \mathcal{N}_c(0, 2AV_X), \tag{3.14}$$

where A is defined as

$$A = \sum_{i=1}^{\infty} \frac{e^{2\sigma G_i}}{R_i^{2b}}. \tag{3.15}$$

Furthermore, after some algebra (Appendix B), V_X can be expressed as

$$V_X = \frac{\mathbb{E}\{E_i\}}{3} + \frac{\mathbb{E}\{\sqrt{E_i E_i'}\cos(\theta_i - \theta_i')\}}{6}, \quad i \geq 1. \tag{3.16}$$

Because the r.v.'s $\{\mathbf{X}_i\}_{i=1}^{\infty}$ are i.i.d., V_X does not depend on i and is only a function of the interferers' signal constellation. For the case of equiprobable symbols and a constellation that is symmetric with respect to the origin of the IQ-plane[3] (e.g., M-PSK and M-QAM), the second right-hand term in (3.16) vanishes and $V_X = \overline{E}/3$, where $\overline{E} = \mathbb{E}\{E_i\}$, $i \geq 1$ is the average symbol energy transmitted by each interfering node.

3.3 Unconditional Interference Distribution

The $\mathcal{P}$-conditioned characterization of $\mathbf{Y}$ given in the previous section is useful when the interfering nodes are immobile or slow-moving. However, it is sometimes more useful to compute the distribution of the interference averaged over the user positions $\mathcal{P}$. Consider, for example, a sensor network (or any packet network) composed of many scattered nodes with a short session life, i.e., each node periodically becomes active, transmits a burst of symbols, and then turns off. Then, the set of *interfering nodes* (i.e., the set of nodes that are transmitting and contributing to the interference) changes often, and so do their distances $\{R_i\}_{i=1}^{\infty}$ and shadowing $\{G_i\}_{i=1}^{\infty}$. In this *dynamic* scenario, it is insightful to average the interference analysis over all possible realizations of user positions $\mathcal{P}$.

We now derive the unconditional distribution of the cumulative interference $\mathbf{Y}$ given in (3.10)-(3.11). It is known that sums of the form of (3.10), where the r.v.'s $\{R_i\}$ correspond to distances in a Poisson point-process and the $\{\mathbf{X}_i\}$ have a CS distribution, belong to the class of stable distributions [8, 10], whose definition and properties were

[3] A constellation is said to be *symmetric with respect to the origin* if for every constellation point (x, y), the point $(-x, -y)$ also belongs to the constellation.

briefly reviewed in Section 1.3. The complex r.v. $\mathbf{X}_i$ defined in (3.11) has in fact a CS distribution, since the phase ϕ_i introduced by the Rayleigh fading is uniform in the interval $[0, 2\pi]$. Then, Appendix C shows that the cumulative interference $\mathbf{Y}$ at the origin has a CS complex stable distribution given by

$$\mathbf{Y} \sim \mathcal{S}_c\left(\alpha_{\mathbf{Y}} = \frac{2}{b},\, \beta_{\mathbf{Y}} = 0,\, \gamma_{\mathbf{Y}} = \lambda\pi C_{2/b}^{-1} e^{2\sigma^2/b^2}\mathbb{E}|X_{ij}|^{2/b}\right), \tag{3.17}$$

where $0 < \alpha_{\mathbf{Y}} < 2$ (or equivalently, $b > 1$), and C_x is given by

$$C_x = \begin{cases} \frac{1-x}{\Gamma(2-x)\cos(\pi x/2)}, & x \neq 1, \\ \frac{2}{\pi}, & x = 1. \end{cases} \tag{3.18}$$

Both real and imaginary components of r.v. $\mathbf{Y}$ have real, symmetric, stable p.d.f.'s, similar to those shown in Figs. 1.1 and 1.3. Using (3.7)-(3.8), we can further express $\mathbb{E}|X_{ij}|^{2/b}$ in (3.17) as

$$\begin{aligned} \mathbb{E}|X_{ij}|^{2/b} &= \mathbb{E}|\alpha_i|^{2/b} \underbrace{\mathbb{E}\left|\sqrt{E_i}\frac{D_i}{T}\cos(\theta_i + \phi_i) + \sqrt{E_i'}\left(1 - \frac{D_i}{T}\right)\cos(\theta_i' + \phi_i)\right|^{2/b}}_{\triangleq \chi(b)} \\ &= \Gamma\left(1 + \frac{1}{b}\right) \cdot \chi(b), \end{aligned} \tag{3.19}$$

where we have used the moment relation for the Rayleigh r.v.'s α_i [19]. Since different interferers i transmit asynchronously and independently, the parameter $\chi(b)$ does not depend on i and is only a function of the amplitude loss exponent b and the interferers' signal constellation. Table 3.1 provides some numerical values for $\mathbb{E}|X_{ij}|^{2/b}$.

3.4 Discussion

The results of this chapter have to be interpreted with care, because of the different types of conditioning involved. In the unconditional case, we let $\mathcal{P}$ be random (i.e., we let $\{R_i\}_{i=1}^{\infty}$ be the random outcomes of an underlying Poisson point process, and $\{G_i\}_{i=1}^{\infty}$

b	$\frac{\mathbb{E}\lvert X_{ij}\rvert^{2/b}}{\overline{E}^{1/b}}$	
	BPSK	QPSK
1.5	0.374	0.385
2	0.423	0.441
3	0.509	0.531
4	0.576	0.599

Table 3.1: $\mathbb{E}|X_{ij}|^{2/b}$ for various amplitude loss exponents b and modulations. Note that for M-PSK modulations, this quantity is proportional to $\overline{E}^{1/b}$, where $\overline{E}$ is the average symbol energy transmitted by each interfering node.

be the random shadowing affecting each interferer). Then, the unconditional interference $\mathbf{Y}$ is *exactly* stable-distributed and given by (3.17).

In the $\mathcal{P}$-conditioned case, however, the positions of the interferers are fixed. Then, A in (3.15) is also a fixed number, and the interference $\mathbf{Y}$ is *approximately* CS Gaussian with total variance $2AV_X$, as given in (3.14). Note that since A in (3.15) depends on the user positions $\mathcal{P}$ (i.e., $\{R_i\}_{i=1}^{\infty}$ and $\{G_i\}_{i=1}^{\infty}$), it can be seen as a r.v. whose value is different for each realization of $\mathcal{P}$. Furthermore, Appendix D shows that r.v. A has a skewed stable distribution given by

$$A \sim \mathcal{S}\left(\alpha_A = \frac{1}{b},\ \beta_A = 1,\ \gamma_A = \lambda\pi C_{1/b}^{-1} e^{2\sigma^2/b^2}\right), \tag{3.20}$$

where $0 < \alpha_A < 1$ (or equivalently, $b > 1$) and C_x is defined in (3.18). This distribution is plotted in Fig. 3.1 for different b and λ.

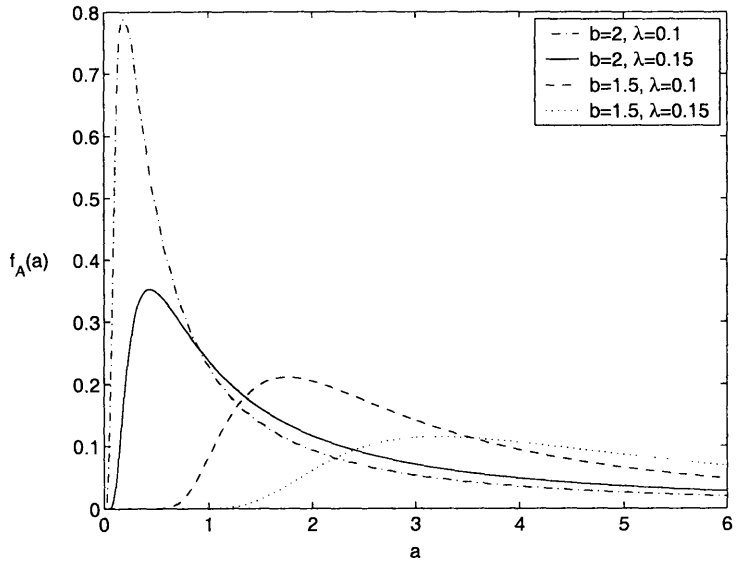

Figure 3.1: P.d.f. of A for different amplitude loss exponents b and interferer densities λ.

Chapter 4

Error Probability

In Chapter 3, we analyzed the distribution of the cumulative interference $\mathbf{Y}$ measured at the origin. In this chapter, we build on those results and characterize the error performance of the probe link, when subject to both interference and thermal noise. We analyze both cases of slow and fast-varying interferer positions.

4.1 Slow-varying Interferer Positions $\mathcal{P}$

As with the interference distribution, in the quasi-static scenario of slow-moving nodes it is insightful to analyze the error probability conditioned on a given realization $\mathcal{P}$ of the distances $\{R_i\}_{i=1}^{\infty}$ and shadowing $\{G_i\}_{i=1}^{\infty}$ of the interferers, as well as on the shadowing G_0 of the probe transmitter node. We denote this conditional error probability by $P_{\mathrm{e}}(G_0, \mathcal{P})$.[1] Again, the fast Rayleigh fading is averaged out in the analysis.

To derive the error probability, we use the results of Section 3.2 for the $\mathcal{P}$-conditioned distribution of the cumulative interference $\mathbf{Y}$. Specifically, using (3.12) and (3.14), the cumulative received signal $\mathbf{Z}$ in (3.9) can be rewritten as

$$\mathbf{Z} = \frac{\alpha_0 e^{\sigma G_0}}{r_0^b}\sqrt{E_0}e^{j\theta_0} + \mathbf{W}', \tag{4.1}$$

[1] The notation $P_{\mathrm{e}}(X, Y)$ is used as a shorthand for $\mathbb{P}\{\text{error}|X, Y\}$.

where

$$\mathbf{W}' = \mathbf{Y} + \mathbf{W} \overset{|\mathcal{P}}{\sim} \mathcal{N}_c(0, 2AV_X + N_0), \tag{4.2}$$

and A was defined in (3.15) as

$$A = \sum_{i=1}^{\infty} \frac{e^{2\sigma G_i}}{R_i^{2b}}. \tag{4.3}$$

We have thus reduced the analysis to a Gaussian problem, where the combined noise $\mathbf{W}'$ is (approximately) Gaussian when conditioned on the location of the interferers. The corresponding error probability $P_e(G_0, \mathcal{P})$ can be found by taking the well-known error probability expressions for detection of linear modulations in the presence of AWGN and fast fading [20–22], but using $2AV_X + N_0$ instead of N_0 for the total noise variance. Note that this substitution is valid for any linear modulation, allowing the traditional results to be extended to include the effect of interference.

In the general case where the probe transmitter employs an arbitrary signal constellation in the IQ-plane, the resulting symbol error probability conditioned on G_0 and $\mathcal{P}$ is given by

$$P_{\mathrm{e}}(G_0, \mathcal{P}) = \sum_{k=1}^{M} p_k \sum_{l \in \mathcal{B}_k} \frac{1}{2\pi} \int_0^{\phi_{k,l}} \left(1 + \frac{w_{k,l}}{4\sin^2(\theta + \psi_{k,l})} \eta_A\right)^{-1} d\theta \tag{4.4}$$

where

$$\eta_A = \frac{e^{2\sigma G_0} \overline{E}_0}{r_0^{2b}(2AV_X + N_0)} \tag{4.5}$$

is the received signal-to-interference-plus-noise ratio (SINR), averaged over the fast fading; M is the constellation size; $\{p_k\}_{k=1}^{M}$ are the symbol probabilities; $\mathcal{B}_k$, $\phi_{k,l}$, $w_{k,l}$, and $\psi_{k,l}$ are the parameters that describe the geometry of the constellation (see Fig. 4.1); $\overline{E}_0 = \mathbb{E}\{E_0\}$ is the average symbol energy transmitted by probe node 0; A and V_X are given in (3.15) and (3.16), respectively. When the probe transmitter employs M-PSK and M-QAM modulations with equiprobable symbols, (4.4) reduces to[2]

$$P_{\mathrm{e}}^{\mathrm{MPSK}}(G_0, \mathcal{P}) = \Lambda\left(\tfrac{M-1}{M}\pi,\, \sin^2\left(\tfrac{\pi}{M}\right)\right) \tag{4.6}$$

[2]For M-QAM, we implicitly assume a square signal constellation with $M = 2^n$ points (n even).

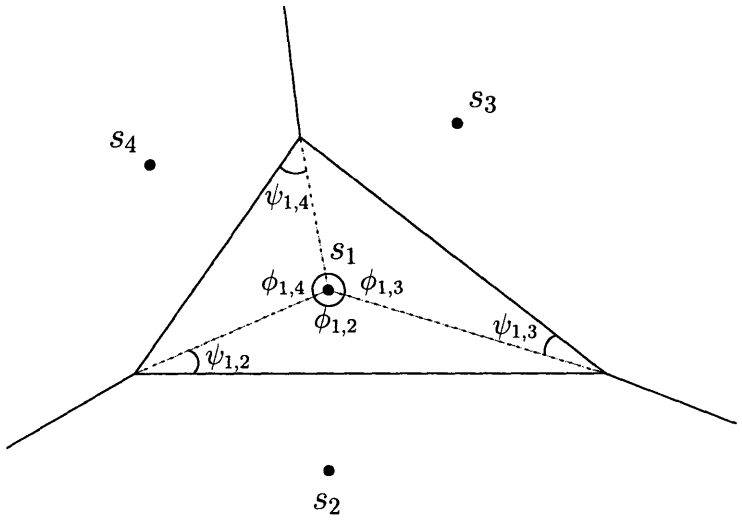

Figure 4.1: Typical decision region associated with symbol s_1. In general, for a constellation with signal points $s_k = |s_k|e^{j\xi_k}$ and $\zeta_k = \frac{|s_k|^2}{\mathrm{E}|s_k|^2}$, $k = 1 \ldots M$, four parameters are required to compute the error probability: $\phi_{k,l}$ and $\psi_{k,l}$ are the angles that describe the decision region corresponding to s_k (as depicted); $\mathcal{B}_k$ is the set consisting of the indices for the signal points that share a decision boundary with s_k (in the example, $\mathcal{B}_1 = \{2, 3, 4\}$); and $w_{k,l} = \zeta_k + \zeta_l - 2\sqrt{\zeta_k \zeta_l}\cos(\xi_k - \xi_l)$.

$$P_{\mathrm{e}}^{\mathrm{MQAM}}(G_0, \mathcal{P}) = 4\left(1 - \tfrac{1}{\sqrt{M}}\right)\Lambda\left(\tfrac{\pi}{2}, \tfrac{3}{2(M-1)}\right) - 4\left(1 - \tfrac{1}{\sqrt{M}}\right)^2 \Lambda\left(\tfrac{\pi}{4}, \tfrac{3}{2(M-1)}\right), \qquad (4.7)$$

where $\Lambda(x, g)$ is given by

$$\Lambda(x, g) = \frac{1}{\pi}\int_0^x \left(1 + \frac{g}{\sin^2\theta}\eta_A\right)^{-1} d\theta. \qquad (4.8)$$

In the general expression given in (4.4)-(4.5), the network interference is accounted for by the term $2AV_X$, where A depends on the interferer spatial distribution and medium propagation characteristics, while V_X depends on the interferer transmission characteristics. Since $2AV_X$ simply adds to N_0, we conclude that the effect of the interference on the error probability is simply to increase the noise level, a fact which is intuitively satisfying. Furthermore, note that the modulation of the interfering nodes affects the term V_X only, while the (possibly different) modulation of the probe transmitter affects the *type* of error probability expression, leading to forms such as (4.6) or (4.7).

In our quasi-static model, the conditional error probability in (4.4) is seen to be a function of the slow-varying user positions and shadowing (i.e., G_0 and $\mathcal{P}$). Since these quantities are random, the error probability itself is a r.v. Then, with some probability, G_0 and $\mathcal{P}$ are such that the error probability of the probe link is above some threshold probability p^*. The system is said to be *in outage*, and the error outage probability is

$$P_{\text{out}}^{\text{e}} = \mathbb{P}_{G_0,\mathcal{P}}(P_{\text{e}}(G_0,\mathcal{P}) > p^*), \tag{4.9}$$

In the case of slow-varying user positions, the error outage probability is a more meaningful metric than the error probability averaged over G_0 and $\mathcal{P}$.

4.2 Fast-varying Interferer Positions $\mathcal{P}$

The $\mathcal{P}$-conditioned error probability given in the previous section is useful when the interfering nodes are immobile or slow-moving. However, there are cases (e.g., packet networks with short session life) where the set of *interfering nodes* changes often, and thus their distances $\{R_i\}_{i=1}^{\infty}$ and shadowing $\{G_i\}_{i=1}^{\infty}$ also change quickly with time. In this dynamic scenario, it is insightful to average the error probability over all possible realizations of interferer positions $\mathcal{P}$. We denote this average error probability by $P_{\text{e}}(G_0)$. Note that we choose not to average out the shadowing G_0 of the probe transmitter, since we have assumed the probe transmitter node is immobile at a deterministic distance r_0 from the origin, and thus G_0 is slow-varying.

To derive the error probability, we use the results of Section 3.3 for the unconditional distribution of the cumulative interference $\mathbf{Y}$. Specifically, using the fact that any stable r.v. is conditionally Gaussian (i.e., Property 1.2), the cumulative interference $\mathbf{Y}$ in (3.17) can expressed as

$$\mathbf{Y} = \sqrt{B}\mathbf{G}, \tag{4.10}$$

where

$$B \sim \mathcal{S}\left(\alpha_B = \frac{1}{b},\ \beta_B = 1,\ \gamma_B = \cos\frac{\pi}{2b}\right) \tag{4.11}$$

$$\mathbf{G} \sim \mathcal{N}_c(0, 2V_G), \quad V_G = 2e^{2\sigma^2/b}\left(\lambda\pi C_{2/b}^{-1}\mathbb{E}|X_{ij}|^{2/b}\right)^b, \quad i \geq 1, \tag{4.12}$$

with $\mathbb{E}|X_{ij}|^{2/b}$ given in (3.19). Conditioning on r.v. B, we then use (3.12) and (4.10) to rewrite the cumulative received signal $\mathbf{Z}$ in (3.9) as

$$\mathbf{Z} = \frac{\alpha_0 e^{\sigma G_0}}{r_0^b}\sqrt{E_0}e^{j\theta_0} + \mathbf{W}',$$

where

$$\mathbf{W}' = \sqrt{B}\mathbf{G} + \mathbf{W} \overset{|B}{\sim} \mathcal{N}_c(0, 2BV_G + N_0). \tag{4.13}$$

We have again reduced the analysis to a Gaussian problem, where the combined noise $\mathbf{W}'$ is a Gaussian r.v. Note that this result was derived without recurring to any approximations – in particular, the Gaussian approximation of (3.13) was not needed here. We merely used the decomposition property of stable r.v.'s.

The corresponding error probability $P_e(G_0)$ can be found by taking the well-known error probability expressions for detection of linear modulations in the presence of AWGN and fast fading [20–22], using $BV_G + N_0/2$ instead of N_0 for the total noise variance, and then averaging over the r.v. B. Note that this procedure is valid for any linear modulation, allowing the traditional results to be extended to include the effect of interference.

In the general case where the probe transmitter employs an arbitrary signal constellation in the IQ-plane, the resulting symbol error probability conditioned on G_0 is given by

$$P_e(G_0) = \sum_{k=1}^{M} p_k \sum_{l\in\mathcal{B}_k} \frac{1}{2\pi}\int_0^{\phi_{k,l}} \mathbb{E}_B\left\{\left(1 + \frac{w_{k,l}}{4\sin^2(\theta+\psi_{k,l})}\eta_B\right)^{-1}\right\} d\theta \tag{4.14}$$

where

$$\eta_B = \frac{e^{2\sigma G_0}\overline{E}_0}{r_0^{2b}(2BV_G + N_0)}; \tag{4.15}$$

M is the constellation size; $\{p_k\}_{k=1}^M$ are the symbol probabilities; $\mathcal{B}_k$, $\phi_{k,l}$, $w_{k,l}$, and $\psi_{k,l}$ are the parameters that describe the geometry of the constellation (see Fig. 4.1);

$\overline{E}_0 = \mathbb{E}\{E_0\}$ is the average symbol energy transmitted by probe node 0; B and V_G are given in (4.11) and (4.12), respectively. When the probe transmitter employs M-PSK and M-QAM modulations with equiprobable symbols, (4.4) reduces to[3]

$$P_{\mathrm{e}}^{\mathrm{MPSK}}(G_0) = \Delta\left(\tfrac{M-1}{M}\pi,\, \sin^2\left(\tfrac{\pi}{M}\right)\right) \tag{4.16}$$

$$P_{\mathrm{e}}^{\mathrm{MQAM}}(G_0) = 4\left(1-\tfrac{1}{\sqrt{M}}\right)\Delta\left(\tfrac{\pi}{2},\, \tfrac{3}{2(M-1)}\right) - 4\left(1-\tfrac{1}{\sqrt{M}}\right)^2\Delta\left(\tfrac{\pi}{4},\, \tfrac{3}{2(M-1)}\right), \tag{4.17}$$

where $\Delta(x, g)$ is given by

$$\Delta(x,g) = \frac{1}{\pi}\int_0^x \mathbb{E}_B\left\{\left(1+\frac{g}{\sin^2\theta}\eta_B\right)^{-1}\right\} d\theta. \tag{4.18}$$

In our dynamic model, the error probability in (4.14) is seen to be a function of the random shadowing G_0 of the probe link, and is therefore random. Then, with some probability, the slow-varying G_0 is such that the error probability of the probe link is above some threshold probability p^*, leading to an *outage*. The corresponding outage probability can thus be defined as

$$P_{\mathrm{out}}^{\mathrm{e}} = \mathbb{P}_{G_0}(P_{\mathrm{e}}(G_0) > p^*), \tag{4.19}$$

In the case of fast-varying user positions, both $P_{\mathrm{e}}(G_0)$ and $P_{\mathrm{out}}^{\mathrm{e}}$ are useful and insightful performance metrics.

4.3 Discussion

In this chapter, we have analyzed the error probability of the probe link when subject to both network self-interference and thermal noise, and considered two distinct cases which differ only in the mobility of the interferers: the static and the dynamic scenario. The results of Section 4.1 for the static case are *approximate*, because they rely on approximation of $\mathbf{X}_i$ by a Gaussian distribution, as shown in (3.13). On the other hand, the results of Section 4.2 for the dynamic case are *exact*, since were derived

[3]For M-QAM, we implicitly assume a square signal constellation with $M = 2^n$ points (n even).

without recurring to the Gaussian approximation.

In addition, note that an *approximation* to error probability $P_e(G_0)$ in (4.14) can be obtained by averaging $P_e(G_0, \mathcal{P})$ in (4.4) over the interferer positions $\mathcal{P}$, i.e., $P_e(G_0) \approx \mathbb{E}_{\mathcal{P}}\{P_e(G_0, \mathcal{P})\}$. Again, this is not exact because the expression for $P_e(G_0, \mathcal{P})$ relies on the Gaussian approximation, while that for $P_e(G_0)$ does not.

We now analyze the dependence of the error performance on the density λ of interfering nodes, and the average symbol energy $\overline{E}$ transmitted by each interfering node. For that purpose, we use (4.4), although (4.14) would lead to similar conclusions. In (4.4), the error probability $P_e(G_0, \mathcal{P})$ implicitly depends on parameters λ and $\overline{E}$ through the product AV_X in the denominator. This is because the dispersion parameter γ_A of the stable r.v. A depends on λ according to (3.20), and V_X is proportional to $\overline{E}$ as in (3.16). The dependence on λ can be made evident by using Property 1.1 to write $AV_X = \lambda^b \widetilde{A} V_X$, where $\widetilde{A}$ is a normalized version of A, independent of λ. We thus conclude that the interference term AV_X is proportional to $\lambda^b \overline{E}$, where $b > 1$ in the proposed model. Clearly, the error performance degrades faster with an increase in the *density* of interferers than with an increase in their *transmitted power*.

The relation between $\overline{E}$ and λ is illustrated in Fig. 4.2, which plots the pairs $(\lambda, \mathsf{INR} = \overline{E}/N_0)$ that lead to a constant $P_{\text{out}}^{\text{e}}$. Clearly, for a fixed error outage probability, there is a tradeoff between the density and energy of the interferers: if $\overline{E}$ (or, equivalently, the INR) increases, λ must decrease, and vice-versa.

4.4 Plots

We now quantify the outage and error probabilities derived in this chapter for several scenarios, and illustrate the dependence of these probabilities on the various parameters involved, such as the signal-to-noise ratio $\mathsf{SNR} = \overline{E}_0/N_0$, the interference-to-noise ratio $\mathsf{INR} = \overline{E}/N_0$, amplitude loss exponent b, interferer density λ, and link length r_0.

Figures 4.3 to 4.4 illustrate the scenario of slow-varying interferer positions $\mathcal{P}$, where the adequate performance metric is the outage probability $P_{\text{out}}^{\text{e}}$ given in (4.9). Two subcases are analyzed:

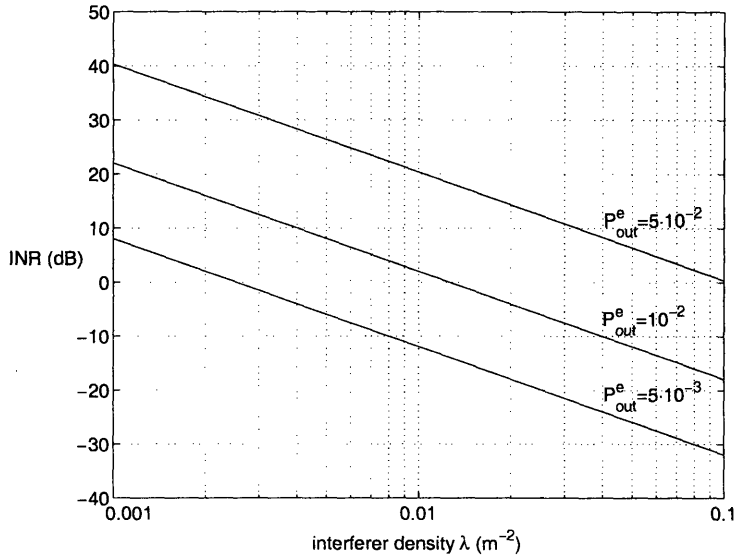

Figure 4.2: $\mathsf{INR} - \lambda$ curves of constant $P_{\text{out}}^{\text{e}}$ (BPSK, $\mathsf{SNR} = 40\,\text{dB}$, $b = 2$, $r_0 = 1\,\text{m}$, $\sigma_s = 10\,\text{dB}$, $p^* = 10^{-2}$).

1. *Heterogeneous network:* The probe transmitter is allowed to use an arbitrary power P_0, different from the common power of the interfering nodes P, and hence $\mathsf{SNR} \neq \mathsf{INR}$ in general. This scenario is useful when the goal is to evaluate the impact of a large number of identical secondary users (e.g., cognitive-radio terminals) on the performance of a primary link.

2. *Homogeneous network:* The probe transmitter and interfering nodes all use the same power, and thus $\mathsf{SNR} = \mathsf{INR}$. This may correspond to a sensor network scenario, where there is a large number of indistinguishable, spatially scattered nodes, with similar transmission characteristics. In such a case, the goal is to evaluate the impact of the cumulative network self-interference on the performance of each sensor node.

Figures 4.5 to 4.6 illustrate the scenario of fast-varying interferer positions $\mathcal{P}$, where the insightful performance metrics are the error probability $P_{\text{e}}(G_0)$ given in (4.14), or the outage probability $P_{\text{out}}^{\text{e}}$ given in (4.19). For simplicity, we choose to plot the former, with $G_0 = 1$ (no shadowing on the main link). As in the case of slow-varying $\mathcal{P}$, we

also analyze the subcases of heterogeneous and homogeneous networks.

For simplicity, the plots assume that all terminals (i.e., the probe transmitter and interfering nodes) use BPSK modulation. To evaluate the corresponding $P_{\text{out}}^{\text{e}}$ and $P_{\text{e}}(G_0)$, we resort to a hybrid approach where we employ the analytical results given in (4.4)-(4.9) and (4.14)-(4.18), but perform a Monte Carlo simulation of all the stable r.v.'s involved (i.e., A and B) according to [23]. As an alternative, numerical integration of those equations is also possible, although computationally more involved. We emphasize that the error probability expressions derived in this chapter completely replace the need for bit-level simulation of the system in order to compute the error performance.

For the heterogeneous case depicted in Figs. 4.3 and 4.5, we conclude that $P_{\text{out}}^{\text{e}}$ and $P_{\text{e}}(G_0)$ deteriorate as λ or INR increase, for a fixed SNR. This is expected because as the interferers' density or transmitted energy increase, the cumulative interference at the probe receiver becomes stronger. Note, however, that in the homogeneous case where $\mathsf{SNR} = \mathsf{INR}$, the error performance improves as we increase the common transmitted power P of the nodes (or equivalently, the SNR), although the gains become marginally small as $P \rightarrow \infty$ (see Figs. 4.4(b) and 4.6(b)). This happens because in the interference-limited regime where $\mathsf{SNR} = \mathsf{INR} \gg 1$, the noise term N_0 in (4.4) and (4.14) becomes irrelevant, and so the SNR in the numerator cancels with the INR in the denominator, making the performance independent of the transmitted power P.

The effect of the amplitude loss exponent b on the error performance, on the other hand, cannot be easily described. As illustrated in Figs. 4.4(a) and 4.6(a), an increase in b may degrade or improve the performance, depending on the value of the link length r_0 and other parameters. This is because b affects both the received signal of interest and the cumulative interference in a non-trivial way – in the former through the term $1/r_0^b$; and in the latter through α_A and γ_A in (3.20), or through α_B, γ_B, and V_G in (4.11)-(4.12).

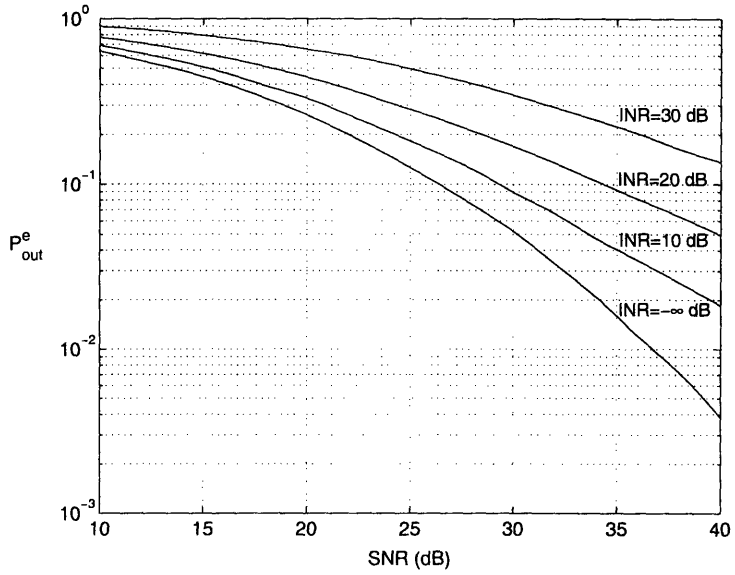

(a) $P^{\mathrm{e}}_{\mathrm{out}}$ versus the SNR of the probe link, for various interference-to-noise ratios INR (BPSK, $b = 2$, $\lambda = 0.01\,\mathrm{m}^{-2}$, $r_0 = 1\,\mathrm{m}$, $\sigma_{\mathrm{s}} = 10\,\mathrm{dB}$, $p^* = 10^{-2}$).

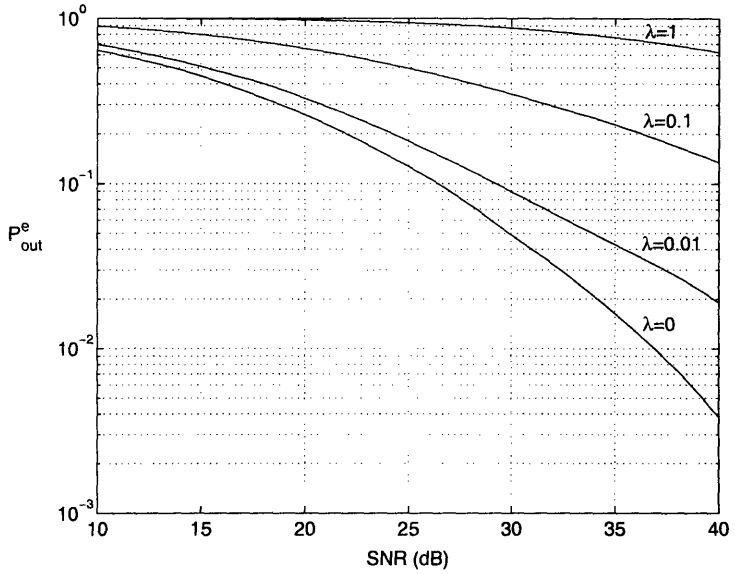

(b) $P^{\mathrm{e}}_{\mathrm{out}}$ versus the SNR of the probe link, for various interferer spatial densities λ in m^{-2} (BPSK, $\mathsf{INR} = 10\,\mathrm{dB}$, $b = 2$, $r_0 = 1\,\mathrm{m}$, $\sigma_{\mathrm{s}} = 10\,\mathrm{dB}$, $p^* = 10^{-2}$).

Figure 4.3: Error outage probability plots for a heterogeneous network (where $\mathsf{SNR} \neq \mathsf{INR}$ in general) and slow-varying interferer positions $\mathcal{P}$.

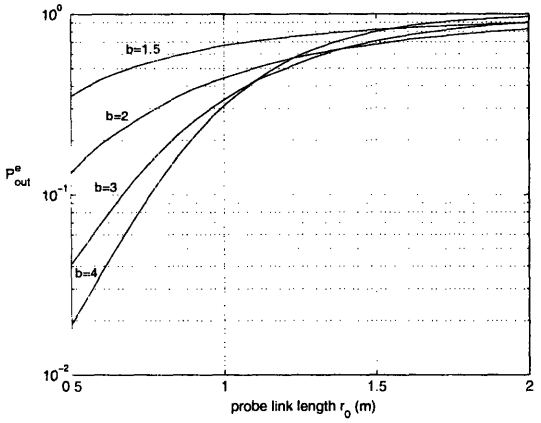

(a) $P_{\text{out}}^{\text{e}}$ versus the length r_0 of the probe link, for various signal loss exponents b (BPSK, $\mathsf{SNR} = \mathsf{INR} = 20\,\text{dB}$, $\lambda = 0.01\,\text{m}^{-2}$, $\sigma_{\text{s}} = 10\,\text{dB}$, $p^* = 10^{-2}$).

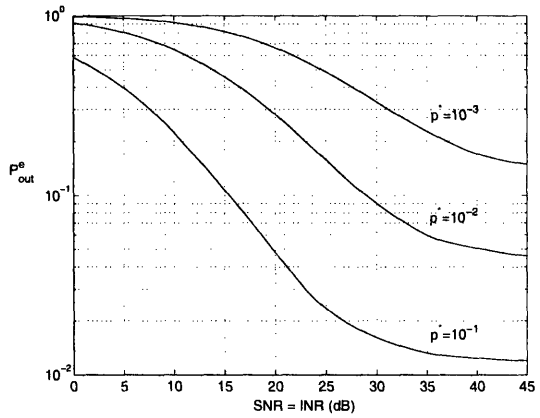

(b) $P_{\text{out}}^{\text{e}}$ versus the SNR, for various threshold probabilities p^* (BPSK, $b = 2$, $\lambda = 10^{-3}\,\text{m}^{-2}$, $\sigma_{\text{s}} = 10\,\text{dB}$).

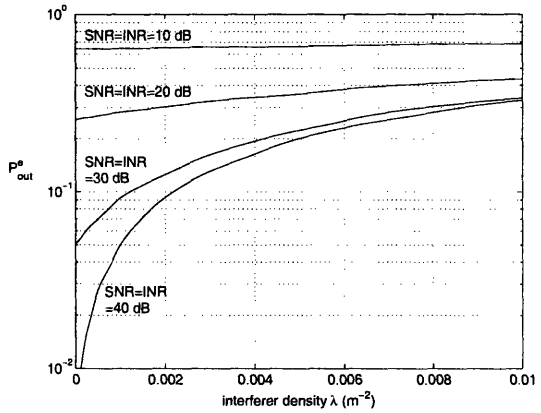

(c) $P_{\text{out}}^{\text{e}}$ versus the interferer spatial density λ, for various SNRs of the probe link (BPSK, $b = 2$, $r_0 = 1\,\text{m}$, $\sigma_{\text{s}} = 10\,\text{dB}$, $p^* = 10^{-2}$).

Figure 4.4: Error outage probability plots for a homogeneous network (where $\mathsf{SNR} = \mathsf{INR}$) and slow-varying interferer positions $\mathcal{P}$.

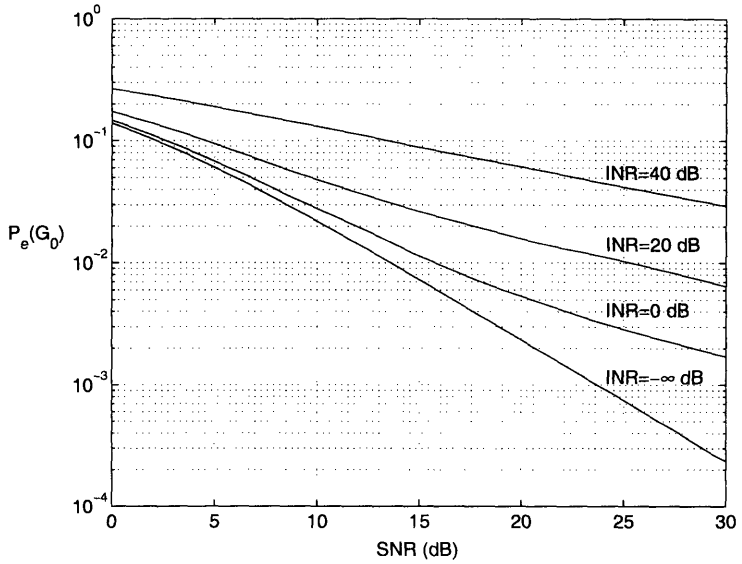

(a) $P_e(G_0)$ versus the SNR of the probe link, for various interferer-to-noise ratios INR (BPSK, $G_0 = 0$, $b = 3$, $\lambda = 0.01\,\mathrm{m}^{-2}$, $r_0 = 1\,\mathrm{m}$, $\sigma_s = 10\,\mathrm{dB}$).

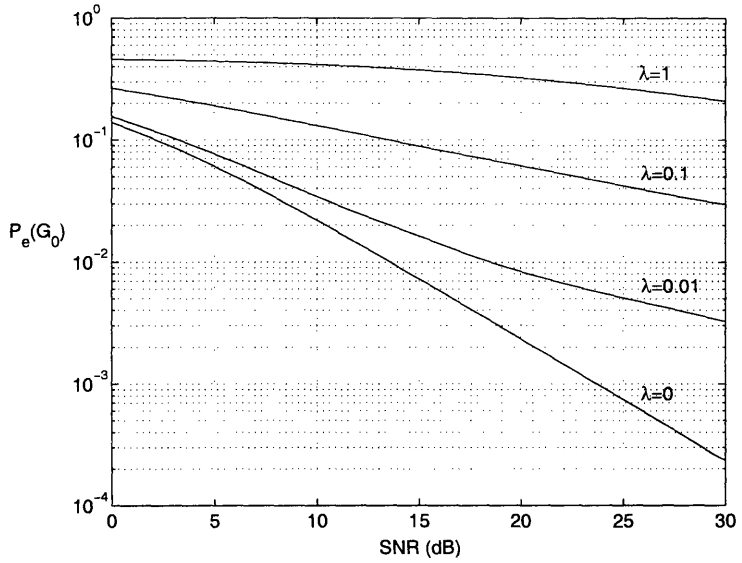

(b) $P_e(G_0)$ versus the SNR of the probe link, for various interferer spatial densities λ in m^{-2} (BPSK, $G_0 = 0$, INR $= 10\,\mathrm{dB}$, $b = 3$, $r_0 = 1\,\mathrm{m}$, $\sigma_s = 10\,\mathrm{dB}$).

Figure 4.5: Average error probability plots for a heterogeneous network (where SNR $\neq$ INR in general) and fast-varying interferer positions $\mathcal{P}$.

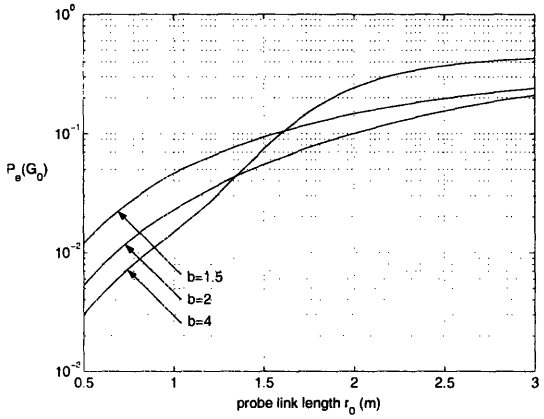

(a) $P_e(G_0)$ versus the length r_0 of the probe link, for various signal loss exponents b (BPSK, $G_0 = 0$, SNR = INR = 20 dB, $\lambda = 0.01\,\mathrm{m}^{-2}$, $\sigma_s = 10\,\mathrm{dB}$).

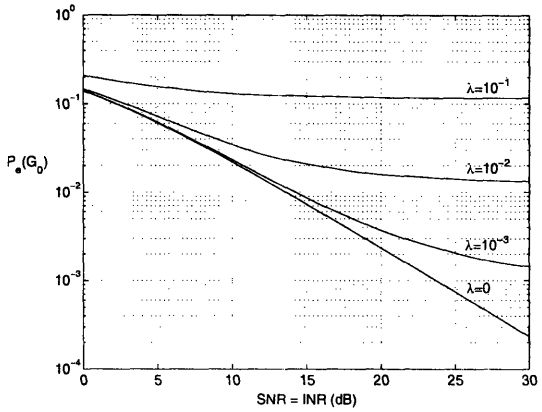

(b) $P_e(G_0)$ versus the SNR, for various interferer densities λ in m^{-2} (BPSK, $G_0 = 0$, $b = 3$, $r_0 = 1\,\mathrm{m}$, $\sigma_s = 10\,\mathrm{dB}$).

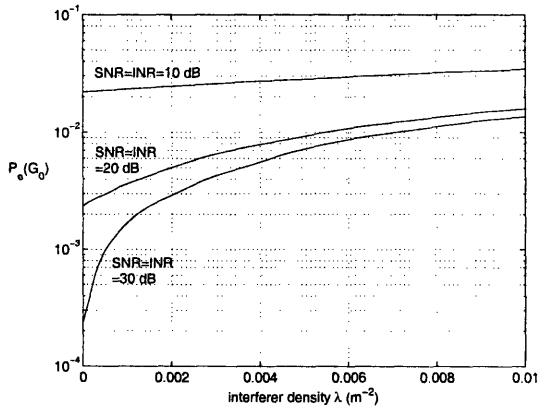

(c) $P_e(G_0)$ versus the interferer spatial density λ, for various SNRs of the probe link (BPSK, $G_0 = 0$, $b = 3$, $r_0 = 1\,\mathrm{m}$, $\sigma_s = 10\,\mathrm{dB}$).

Figure 4.6: Average error probability plots for a homogeneous network (where SNR = INR) and fast-varying interferer positions $\mathcal{P}$.

Chapter 5

Channel Capacity

The channel capacity, a notion introduced by Shannon in the late 1940s, is an important and useful characterization of a communication system. It corresponds to the maximum rate that can be transmitted over a given channel, with asymptotically small error probability. The capacity is thus a fundamental limit on the performance achievable on a channel. Its definition is based on the notion of mutual information between the input and output of a channel. More precisely, the capacity of a memoryless channel is the maximum mutual information $I(X;Y)$ between channel input X and output Y, where the maximization is over all possible input probability distributions that satisfy a given energy constraint. More details on mutual information, channel capacity, and related coding theorems can be found in [24].

In this chapter, we build on the previous results and analyze the capacity of the link between the probe transmitter and probe receiver, when subject to both network self-interference and AWGN thermal noise. We will refer to this link as the *probe channel*. Unlike the simple AWGN channel, here the capacity is not given by a single formula, but depends on the assumptions we make about the shadowing, multipath fading, and interferer mobility. In what follows, we perform the analysis assuming that the location $\{R_i\}_{i=1}^{\infty}$ and shadowing $\{G_i\}_{i=1}^{\infty}$ of the interferers *remain constant for all time* (i.e., the $\mathcal{P}$-conditioned case), as well as the shadowing G_0 affecting the probe transmitter node. This models a *quasi-static* scenario where the movement of the nodes

during the interval of interest is negligible.[1] The Rayleigh fading, on the other hand, is averaged out in the analysis, due to its fast nature. As we will see, these assumptions naturally lead to a characterization of the channel capacity in terms of a *capacity outage probability.*

The channel capacity depends also on what is known about the channel at the probe transmitter and receiver. For consistency with previous chapters, we assume the probe receiver can perfectly estimate the Rayleigh fading (α_0 and ϕ_0) affecting its own link. The probe transmitter, on the other hand, only has access to the probabilistic description of the channel. This corresponds to the *receiver channel side information (CSI)* scenario.

5.1 Capacity Outage Probability

We start with the complex baseband characterization of the probe channel, which can be written as

$$\mathbf{Z} = \frac{\alpha_0 e^{\sigma G_0}}{r_0^b}\mathbf{S} + \mathbf{W}', \tag{5.1}$$

where $\mathbf{S}$ is the (complex) channel input, $\mathbf{Z}$ is the (complex) channel output, and the distribution of $\mathbf{W}'$ is given by

$$\mathbf{W}' \overset{|\mathcal{P}}{\sim} \mathcal{N}_c(0, 2AV_X + N_0),$$

with

$$A = \sum_{i=1}^{\infty} \frac{e^{2\sigma G_i}}{R_i^{2b}}. \tag{5.2}$$

These are essentially the same baseband equations as those given in (4.1)-(4.3), but where the transmitted constellation symbol $\sqrt{E_0}e^{j\theta_0}$ has been replaced by a general input symbol $\mathbf{S}$, with an arbitrary distribution $f_{\mathbf{S}}(s)$. This is emphasizes the fact that we need to maximize the mutual information over all possible input distributions $f_{\mathbf{S}}(s)$, and thus cannot restrict $\mathbf{S}$ to belong to M-PSK or M-QAM constellations. In addition, we

[1] Unless otherwise indicated, we implicitly assume conditioning on $\mathcal{P}$ in the following.

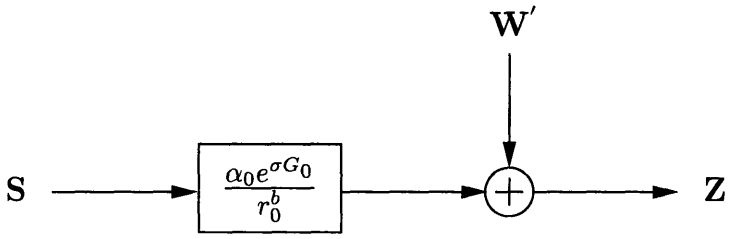

Figure 5.1: Channel model for capacity analysis.

impose an average energy constraint on the input symbol by requiring that $\mathbb{E}|\mathbf{S}|^2 \leq \overline{E}_{\mathbf{S}}$.

Note that because of the conditioning on G_0 and $\mathcal{P}$, equations (5.1)-(5.2) describe a simple Gaussian channel depicted schematically in Fig. 5.1. The capacity of this energy-constrained, fast fading channel with receiver CSI can be written as [25]

$$C = \max_{f_{\mathbf{S}}:\mathbb{E}|\mathbf{S}|^2 \leq \overline{E}_{\mathbf{S}}} I(\mathbf{S};\mathbf{Z}|\alpha_0).$$

The optimal input distribution that maximizes the mutual information is therefore $\mathcal{N}_c(0,\overline{E}_{\mathbf{S}})$. With this input distribution,

$$\begin{aligned} I(\mathbf{S};\mathbf{Z}|\alpha_0 = \hat{\alpha_0}) &= 2 \times \frac{1}{2}\log_2\left(1 + \frac{\frac{\hat{\alpha_0}^2 e^{2\sigma G_0}}{r_0^{2b}}\overline{E}_{\mathbf{S}}}{\mathbb{E}|\mathbf{W}'|^2}\right) \\ &= \log_2\left(1 + \frac{\hat{\alpha_0}^2 e^{2\sigma G_0}\overline{E}_{\mathbf{S}}}{r_0^{2b}(2AV_X + N_0)}\right) \quad \text{bits/complex symbol.} \end{aligned}$$

Using the fact that $I(\mathbf{S};\mathbf{Z}|\alpha_0) = \mathbb{E}_{\hat{\alpha_0}}\{I(\mathbf{S};\mathbf{Z}|\alpha_0 = \hat{\alpha_0})\}$, we obtain the capacity of the channel as

$$C(G_0,\mathcal{P}) = \mathbb{E}_{\alpha_0}\left\{\log_2\left(1 + \frac{\alpha_0^2 e^{2\sigma G_0}\overline{E}_{\mathbf{S}}}{r_0^{2b}(2AV_X + N_0)}\right)\middle| G_0, A\right\} \quad \text{bits/complex symbol,} \quad (5.3)$$

where we have explicitly indicated the conditioning of C on the random user positions and shadowing. Using the fact that $\alpha_0^2 \sim \mathcal{E}xp(\sqrt{2})$,[2] we can further express (5.3) in

[2]The parameter $\lambda = \sqrt{2}$ ensures that the fading has unit power gain, i.e., $\mathbb{E}\{\alpha_0^2\} = 1$.

terms of the exponential integral function [26] as

$$C(G_0, \mathcal{P}) = -\frac{\exp\left(\frac{\sqrt{2}}{\eta}\right)}{\ln(2)} \mathrm{Ei}\left(-\frac{\sqrt{2}}{\eta}\right) \quad \text{bits/complex symbol,} \tag{5.4}$$

where

$$\eta = \frac{e^{2\sigma G_0} \overline{E}_{\mathbf{S}}}{r_0^{2b}(2AV_X + N_0)} \tag{5.5}$$

is the received signal-to-interference-plus-noise ratio (SINR), averaged over the fast fading.

In our quasi-static model, the maximum rate of reliable communication for a given realization of G_0 and $\mathcal{P}$ is given by (5.4)-(5.5). This quantity is a function of the random user positions and shadowing, and is therefore random. Then, with some probability, G_0 and $\mathcal{P}$ are such that the capacity is below the transmission rate R, thus making the channel unusable for communication with arbitrarily low error probability. The system is said to be *in outage*, and the capacity outage probability is

$$P_{\text{out}}^{\text{c}} = \mathbb{P}_{G_0,\mathcal{P}}\{C(G_0, \mathcal{P}) < R\}, \tag{5.6}$$

or, substituting (5.4)-(5.5) into (5.6),

$$P_{\text{out}}^{\text{c}} = \mathbb{P}_{\eta}\left\{-\frac{\exp\left(\frac{\sqrt{2}}{\eta}\right)}{\ln(2)} \mathrm{Ei}\left(-\frac{\sqrt{2}}{\eta}\right) < R\right\}. \tag{5.7}$$

5.2 Plots

Figures 5.2 and 5.3 quantify the capacity error probability derived in this chapter, and illustrate its dependence on the various parameters involved, such as the signal-to-noise ratio $\mathsf{SNR} = \overline{E}_{\mathbf{S}}/N_0$, the interference-to-noise ratio $\mathsf{INR} = \overline{E}/N_0$, and spatial density λ of the interferers. For simplicity, the plots assume that all interfering nodes transmit equiprobable symbols, belonging to a constellation that is symmetric with respect to the origin of the IQ-plane (e.g., M-PSK and M-QAM). In this particular case, $V_X = \overline{E}/3$

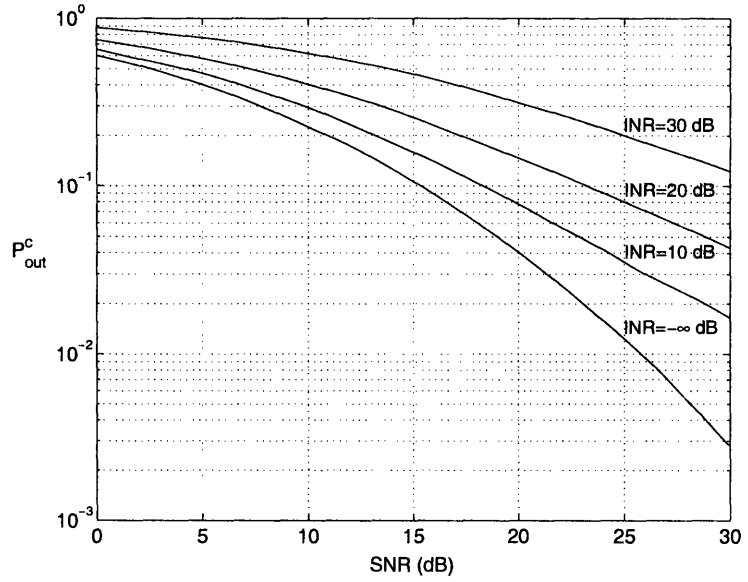

Figure 5.2: Capacity outage probability P^{c}_{out} versus the SNR of the probe link, for various interferer-to-noise ratios INR ($R = 1\,\text{bit/complex symbol}$, $\lambda = 0.01\,\text{m}^{-2}$, $b = 2$, $r_0 = 1\,\text{m}$, $\sigma_s = 10\,\text{dB}$).

and (5.5) reduces to

$$\eta = \frac{e^{2\sigma G_0}\mathsf{SNR}}{r_0^{2b}\left(\frac{2A}{3}\mathsf{INR}+1\right)}. \tag{5.8}$$

To evaluate the corresponding P^{c}_{out}, we proceed as in Section 4.4. Specifically, we resort to a hybrid approach where we employ the analytical result given in (5.7)-(5.8), but perform a Monte Carlo simulation of the stable r.v. A according to [23]. As an alternative, numerical integration of (5.7)-(5.8) is also possible, although computationally more involved. Again, the expressions derived in this chapter completely replace the need for bit-level simulation of the system in order to compute the capacity metrics.

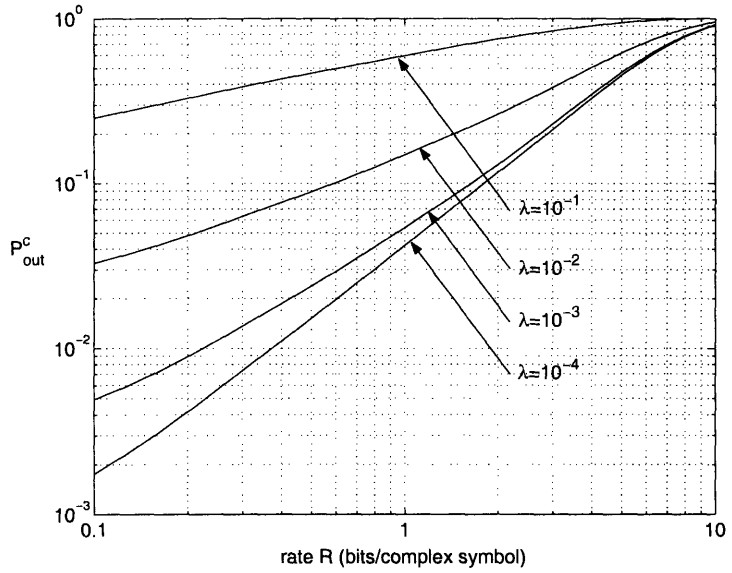

Figure 5.3: Capacity outage probability $P_{\text{out}}^{\text{c}}$ versus the transmission rate R, for various interferer spatial densities λ in m^{-2} ($\mathsf{SNR} = \mathsf{INR} = 20\,\text{dB}$, $b = 2$, $r_0 = 1\,\text{m}$, $\sigma_s = 10\,\text{dB}$).

Chapter 6

Spectral Characterization of the Interference

The spectral occupancy and composition of the cumulative interference in a network is an important consideration in the design of wireless networks. In sensor or mobile networks, it is often desirable to know the spectral properties of the cumulative interference generated by all the spatially scattered nodes. Due to the scarcity of the electromagnetic spectrum, the communications designer has to ensure that the network's spectral emission does not cause interference to other networks operating in the same frequency band. In many commercial applications, the networks have to operate under the restrictions imposed by a regulatory agency (e.g. the FCC), which often assume the form of spectral masks. In military applications, on the other hand, the goal is ensure that the presence of deployed networks is not detected by the enemy. If, for example, a sensor network is to be deployed in enemy territory, then the knowledge of the cumulative network emission measured any location in space is essential for the design of a covert system.

In this chapter, we analyze the power spectral density (PSD) of the cumulative interference process $\mathbf{Y}(t)$, measured at the origin of the two-dimensional plane. The spectral characteristics of $\mathbf{Y}(t)$ can be inferred from the knowledge of its PSD. We perform the analysis assuming that the location $\{R_i\}_{i=1}^{\infty}$ and shadowing $\{G_i\}_{i=1}^{\infty}$ of the

interferers *remain constant for all time*, i.e., the $\mathcal{P}$-conditioned case.[1] This models a *quasi-static* scenario where the movement of the nodes during the interval of interest is negligible. Furthermore, it will enable the derivation of a spectral outage probability – a more meaningful metric than the PSD averaged over $\mathcal{P}$, in the case of slow-varying $\mathcal{P}$. Because of its fast nature, the Rayleigh fading is averaged out in the analysis.

6.1 Power Spectral Density of the Interference

The cumulative interference at the origin can be characterized by the complex baseband random process $\mathbf{Y}(t)$, defined as

$$\mathbf{Y}(t) = \sum_{i=1}^{\infty} \mathbf{Y}_i(t), \tag{6.1}$$

where $\mathbf{Y}_i(t)$ is the received process associated with interferer i,

$$\mathbf{Y}_i(t) = \sum_{n=-\infty}^{+\infty} \frac{\alpha_{i,n} e^{j\phi_{i,n}} e^{\sigma G_i}}{R_i^b} \mathbf{a}_{i,n} p(t - nT - D_i), \quad -\infty < t < +\infty. \tag{6.2}$$

This is essentially the same model employed in the previous chapters, but with the inclusion of a generic shaping pulse $p(t)$, which is normalized to have unit energy, i.e., $\|p(t)\|^2 = 1$. In Chapters 3-5, we implicitly assumed $p(t)$ was rectangular, since the spectral characteristics of the interference were not of concern. Here, however, our goal is to analyze the spectral properties of $\mathbf{Y}(t)$, so we incorporate in the model a generic, real, baseband pulse $p(t)$, defined over all time $\infty < t < +\infty$. Also, since in this chapter we are only interested in the cumulative effect of the interferers, we can ignore the existence of the probe link introduced in Chapter 2.

The sequence $\{\mathbf{a}_{i,n}\}_{n=-\infty}^{+\infty}$ in (6.2) represents the stream of complex symbols transmitted by interferer i, assumed i.i.d. in n and zero-mean, for simplicity. The type of constellation employed by the interferers (e.g., M-PSK or M-QAM) is captured by the statistics of the symbols $\{\mathbf{a}_{i,n}\}$.[2] Each interferer i is also affected by a se-

[1] Unless otherwise indicated, we implicitly assume conditioning on $\mathcal{P}$ in the following.

[2] Note that each symbol $\mathbf{a}_{i,n}$ can be represented in the IQ-plane as the constellation

quence $\{\alpha_{i,n}e^{j\phi_{i,n}}\}_{n=-\infty}^{+\infty}$ with arbitrary autocorrelation in n, which models the fast Rayleigh fading assumed in previous chapters. Furthermore, in what follows we carry the analysis in complex baseband, although it can be trivially extended to passband frequencies.

The random processes $\mathbf{Y}_i(t)$ and $\mathbf{Y}(t)$ can be shown to be WSS: first, if we deterministically set D_i to zero in (6.2), the resulting process $\widetilde{\mathbf{Y}}_i(t)$ is WSCS [27]; then, since $\mathbf{Y}_i(t) = \widetilde{\mathbf{Y}}_i(t - D_i)$, where $D_i \sim \mathcal{U}(0, T)$ and independent everything else, it follows that $\mathbf{Y}_i(t)$ is WSS and thus the cumulative process $\mathbf{Y}(t)$ is also WSS.

We now wish to compute the PSD of the process $\mathbf{Y}(t)$, defined as

$$S_{\mathbf{Y}}(f) = \mathcal{F}\{R_{\mathbf{Y}}(\tau)\},$$

where $R_{\mathbf{Y}}(\tau) = \mathbb{E}\{\mathbf{Y}(t)\mathbf{Y}^*(t+\tau)\}$ is the autocorrelation function of $\mathbf{Y}(t)$. Because the processes $\mathbf{Y}_i(t)$ associated with different interferers i are statistically independent, we can write

$$S_{\mathbf{Y}}(f) = \sum_{i=1}^{\infty} S_{\mathbf{Y}_i}(f). \tag{6.3}$$

We then define $\widetilde{\mathbf{a}}_{i,n} = \mathbf{a}_{i,n}\alpha_{i,n}e^{j\phi_{i,n}}e^{\sigma G_i}/R_i^b$ and rewrite (6.2) as $\mathbf{Y}_i(t) = \sum_{n=-\infty}^{+\infty} \widetilde{\mathbf{a}}_{i,n}p(t - nT - D_i)$, whose PSD is equal to [28, 29] $|P(f)|^2\mathbb{E}|\widetilde{\mathbf{a}}_{i,n}|^2/T$, since the sequence $\{\widetilde{\mathbf{a}}_{i,n}\}$ is i.i.d. zero-mean. Conditioned on $\mathcal{P}$, both R_i and G_i are constant, so $\mathbb{E}|\widetilde{\mathbf{a}}_{i,n}|^2 = \mathbb{E}|\mathbf{a}_{i,n}|^2e^{2\sigma G_i}/R_i^{2b}$ and thus

$$S_{\mathbf{Y}_i}(f) = \frac{|P(f)|^2}{T}\mathbb{E}|\mathbf{a}_{i,n}|^2\frac{e^{2\sigma G_i}}{R_i^{2b}}. \tag{6.4}$$

Combining (6.1) and (6.4), we finally obtain the desired PSD of the conditional cumulative interference $\mathbf{Y}(t)$,

$$S_{\mathbf{Y}}(f, \mathcal{P}) = \frac{|P(f)|^2}{T}\mathbb{E}|\mathbf{a}_{i,n}|^2 A, \tag{6.5}$$

---

point $\sqrt{E_{i,n}}e^{j\theta_{i,n}}$.

where A was defined in (3.15) to be

$$A = \sum_{i=1}^{\infty} \frac{e^{2\sigma G_i}}{R_i^{2b}}. \tag{6.6}$$

Note in (6.5) that we have explicitly indicated the conditioning of $S_{\mathbf{Y}}$ on the random user positions and shadowing, $\mathcal{P}$. Since A depends on $\mathcal{P}$ (i.e., $\{R_i\}_{i=1}^{\infty}$ and $\{G_i\}_{i=1}^{\infty}$), for each realization of $\mathcal{P}$ we obtain a realization of the cumulative spectrum $S_{\mathbf{Y}}(f, \mathcal{P})$. Then, for a fixed f, $S_{\mathbf{Y}}(f, \mathcal{P})$ can be seen as r.v. whose value is different for each realization of user positions and shadowing.[3] Finally, we recall that A, when seen as a r.v., has a skewed stable distribution given by (3.20), and repeated here for convenience:

$$A \sim \mathcal{S}\left(\alpha_A = \frac{1}{b},\, \beta_A = 1,\, \gamma_A = \lambda \pi C_{1/b}^{-1} e^{2\sigma^2/b^2}\right). \tag{6.7}$$

6.2 Spectral Outage Probability

In our quasi-static scenario, the PSD of the cumulative interference, $S_{\mathbf{Y}}(f, \mathcal{P})$, is a function of the random user positions and shadowing, $\mathcal{P}$. Then, with some probability, $\mathcal{P}$ is such that the interference spectrum is too high in some frequency band of interest, thus making that band unusable for communications. This leads to the concept of *spectral outage probability* (SOP), which we denote by $P_{\text{out}}^{\text{s}}(f)$ and generally define as

$$P_{\text{out}}^{\text{s}}(f) = \mathbb{P}_{\mathcal{P}}\{S_{\mathbf{Y}}(f, \mathcal{P}) > m(f)\}, \tag{6.8}$$

where $S_{\mathbf{Y}}(f, \mathcal{P})$ is the (random) PSD of the cumulative interference process $\mathbf{Y}(t)$, and $m(f)$ is some spectral mask determining the outage threshold at the receiver. The SOP is a frequency-dependent quantity and, in the case of slow-varying user positions $\mathcal{P}$, is a more meaningful metric than the PSD averaged over $\mathcal{P}$. Note that this definition is applicable in general to any interference model: the spectral outage probability $P_{\text{out}}^{\text{s}}(f)$

[3] $S_{\mathbf{Y}}(f, \mathcal{P})$ is in fact a random process whose sample paths evolve in *frequency* instead of *time*. For each realization $\mathcal{P} = \mathcal{P}_0$, we obtain a sample path $S_{\mathbf{Y}}(f, \mathcal{P}_0)$ that is a function of f; for a fixed frequency $f = f_0$, $S_{\mathbf{Y}}(f_0, \mathcal{P})$ is a r.v.

represents the probability that the PSD of the cumulative interference, measured at an arbitrary location in the plane and at a particular frequency, exceeds some predetermined mask.

The function $m(f)$ may correspond to a frequency-dependent mask imposed by regulatory agencies, with the purpose of limiting the cumulative interference generated by a network, and protecting other services that operate in dedicated bands (e.g., GPS, public safety, and cellular systems). Current regulations and standards (e.g., FCC Part 15 or IEEE 802.11) impose a spectral mask on the *transmitted* PSD, and the type of mask often depends on the environment in which the devices are operated (e.g., indoor or outdoor). However, the transmitted PSD is usually not representative of the cumulative PSD at the receiver, due to random propagation effects (shadowing and multipath fading), and accumulation of signals from randomly located interfering nodes. In this chapter, we propose a radically different approach: the mask $m(f)$ in (6.8) represents the outage threshold with respect to the interference PSD *accumulated at the receiver*, not the PSD at the transmitter (this follows from the fact that $S_{\mathbf{Y}}(f, \mathcal{P})$ is measured at an arbitrary position in the plane, where a probe receiver could be located). The received interference spectrum $S_{\mathbf{Y}}(f, \mathcal{P})$ and the corresponding $P_{\text{out}}^{\text{s}}(f)$ can be used to control the network interference more effectively, since they consider the cumulative effect of all interfering nodes at an arbitrary receiver location, and incorporate both random propagation effects and random interferer positions. Furthermore, the use of different masks for indoor or outdoor environments is now unnecessary, since the environment is already accounted for in our model by parameters such as the amplitude loss exponent b, the interferer density λ, or the shadowing coefficient σ_{s}.

For the interference model we have assumed in (6.1)-(6.2), $P_{\text{out}}^{\text{s}}(f)$ can be computed by substituting (6.5) into (6.8), which leads to

$$\begin{aligned} P_{\text{out}}^{\text{s}}(f) &= \mathbb{P}\left\{ A > \frac{Tm(f)}{\mathbb{E}|\mathbf{a}_{i,n}|^2 |P(f)|^2} \right\} \\ &= 1 - F_A\left(\frac{Tm(f)}{\mathbb{E}|\mathbf{a}_{i,n}|^2 |P(f)|^2} \right), \end{aligned} \tag{6.9}$$

where $F_A(\cdot)$ is the c.d.f. of the stable r.v. A, whose p.d.f. is given in (6.7). Since

$F_A(\cdot)$ cannot be expressed in closed form except in the case where $b = 2$, (6.9) must be computed numerically for each frequency f. In the case of slow-varying user positions, the spectral outage probability is a more meaningful metric than the PSD averaged over $\mathcal{P}$.

6.3 Discussion

Up until Chapter 6, we considered the case where the modulation of the interfering nodes and the (possibly different) modulation of the probe transmitter are all *linear*, and analyzed the error performance and capacity of the probe link, when subject to interference and noise. In many cases, however, it is desirable to consider the general case where the interfering nodes and probe link employ different types of modulation, symbol rates, and carrier frequencies. For example, we may be interested in evaluating the impact of the interference generated by a scattered sensor network on a primary link, where the sensor nodes transmit at carrier frequency f_0 using low data rate BPSK, while the primary nodes transmit in the same frequency band at carrier frequency f_1, using high data rate 16-FSK. Because the error and capacity analysis is highly dependent on the characteristics of the primary link affected by the interference, the results in the previous chapters do not hold directly. However, all the spectral characterization results in this chapter apply without change, since they depend on the interfering nodes, not on the particularities of link subject to the interference. This reasoning justifies why interference control can be better accomplished through spectral restrictions (e.g. a maximum spectral outage probability), rather than restrictions in the error or capacity performance (e.g. a maximum error or capacity outage probability).

6.4 Plots

We now quantify the spectral densities and outage probabilities derived in previous sections, and illustrate their dependence on the various parameters involved, such as the pulse shape $p(t)$, spectral mask $m(f)$, transmitted power $P = \frac{\mathbb{E}|\mathbf{a}_{i,n}|^2}{T}$, and density λ

of the interfering nodes.

From Figs. 6.1 and 6.2, we see that the outage probability $P_{\text{out}}^{\text{s}}(f)$ is a frequency-dependent quantity which resembles the spectrum $|P(f)|$ of the transmitted pulse. In fact, $P_{\text{out}}^{\text{s}}(f)$ is a nonlinear function of $|P(f)|$, where the nonlinearity is determined by the c.d.f. $F_A(\cdot)$ of the stable r.v. A, as shown in (6.9). Since $P_{\text{out}}^{\text{s}}(f)$ incorporates both $P(f)$ and $m(f)$, it quantifies how well the shape of the transmitted pulse in a network is matched to the spectral regulations in the area, as imposed by regulatory agencies. The spectral outage can also be used for pulse shape design, i.e., the baseband pulse $p(t)$ and transmitted power P should be such that $\max_f P_{\text{out}}^{\text{s}}(f) \leq p^*$, where p^* is some target outage probability which should be satisfied at all frequencies (e.g., in commercial applications, to ensure that the restrictions imposed by a regulatory agency are met; or in military applications, to guarantee that the presence of a surveillance network deployed in enemy territory is not detected).

Figures 6.3 and 6.4 illustrate the dependence of the outage probability $P_{\text{out}}^{\text{s}}(f)$ on the interferers' transmitted power P and spatial density λ. Specifically, as P or λ increase, the cumulative interference becomes stronger, and thus $P_{\text{out}}^{\text{s}}(f)$ deteriorates at all frequencies, approaching the maximum value of 1.

6.5 Generalizations

The results derived in this chapter hold without change if the following generalizations are made: 1) the sequence $\{\mathbf{a}_{i,n}\}_{n=-\infty}^{+\infty}$ of symbols transmitted by interferer i is *uncorrelated* in n and zero-mean; and 2) the fading sequence $\{\alpha_{i,n}e^{j\phi_{i,n}}\}_{n=-\infty}^{+\infty}$, which models the fast fading affecting interferer i, can have an *arbitrary* joint distribution in n – in particular, it needs not be Rayleigh distributed. These generalizations arise from the fact that to derive the PSD, only the first and second-order statistics of $\{\mathbf{a}_{i,n}\}$, $\{\alpha_{i,n}\}$, and $\{\phi_{i,n}\}$ are required, not their full characterization.

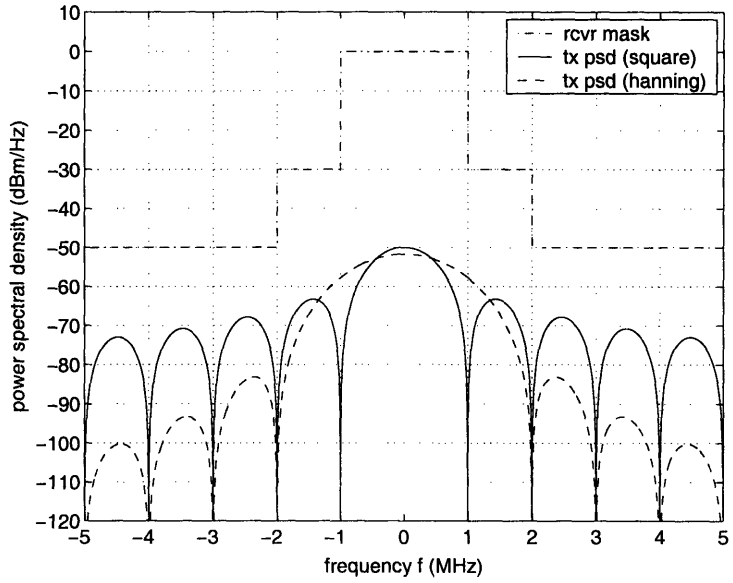

(a) PSD of the transmitted interfering signal versus frequency (bottom), for various pulse shapes $p(t)$. The square and Hanning pulses are normalized so that the transmitted signals have the same power P. Also shown is a piecewise-constant spectral mask $m(f)$ (top), similar to an IEEE 802.11b mask, which determines the outage threshold at the receiver.

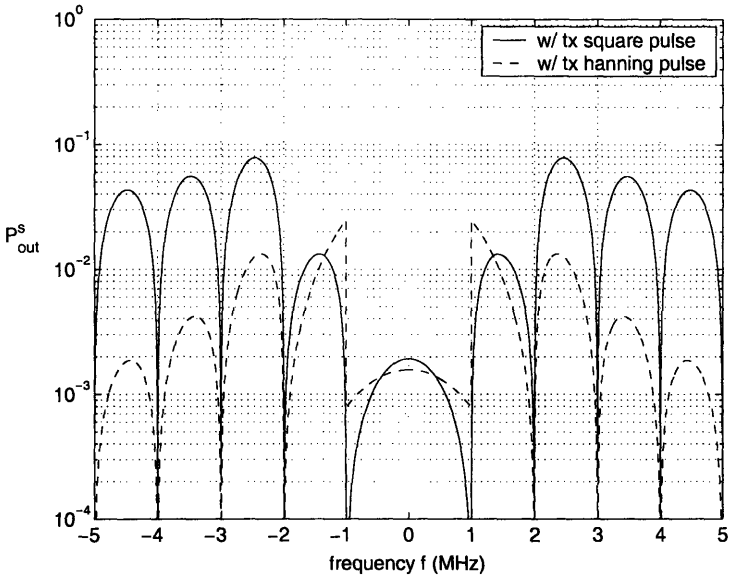

(b) Spectral outage probability $P^{\mathrm{s}}_{\mathrm{out}}(f)$ versus frequency, for the piecewise-constant mask $m(f)$ shown in (a).

Figure 6.1: Effect of the transmitted baseband pulse shape $p(t)$ on the PSD and the outage probability $P^{\mathrm{s}}_{\mathrm{out}}(f)$ ($P = 10\,\mathrm{dBm}$, $T = 10^{-6}\,\mathrm{s}$, $\lambda = 0.1\,\mathrm{m}^{-2}$, $b = 2$, $\sigma_{\mathrm{s}} = 10\,\mathrm{dB}$).

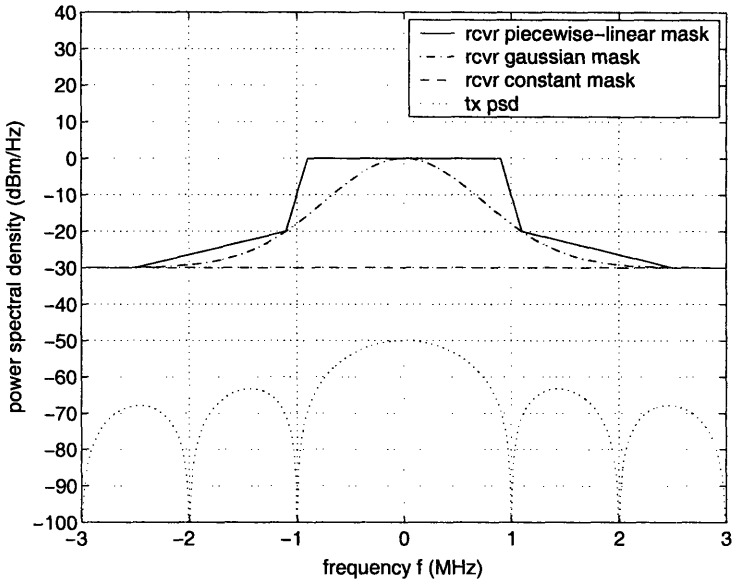

(a) Plot of various spectral masks $m(f)$ which define the outage threshold at the receiver (top). The piecewise-linear mask is similar to those employed in IEEE 802.11a/g systems. Also shown is the PSD of the transmitted interfering signal versus frequency (bottom).

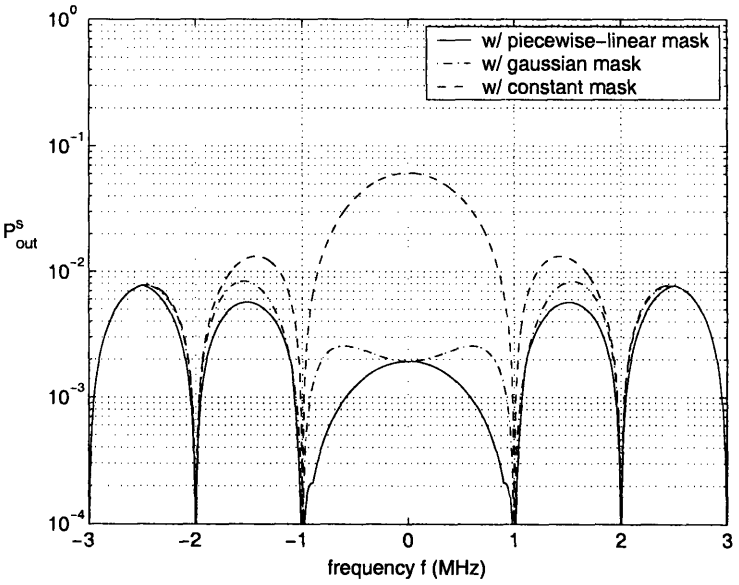

(b) Spectral outage probability $P^{\mathrm{s}}_{\mathrm{out}}(f)$ versus frequency, for the various masks $m(f)$ shown in (a).

Figure 6.2: Effect of the spectral mask shape $m(f)$ on the outage probability $P^{\mathrm{s}}_{\mathrm{out}}(f)$ (square $p(t)$, $P = 10\,\mathrm{dBm}$, $T = 10^{-6}\,\mathrm{s}$, $\lambda = 0.1\,\mathrm{m}^{-2}$, $b = 2$, $\sigma_{\mathrm{s}} = 10\,\mathrm{dB}$).

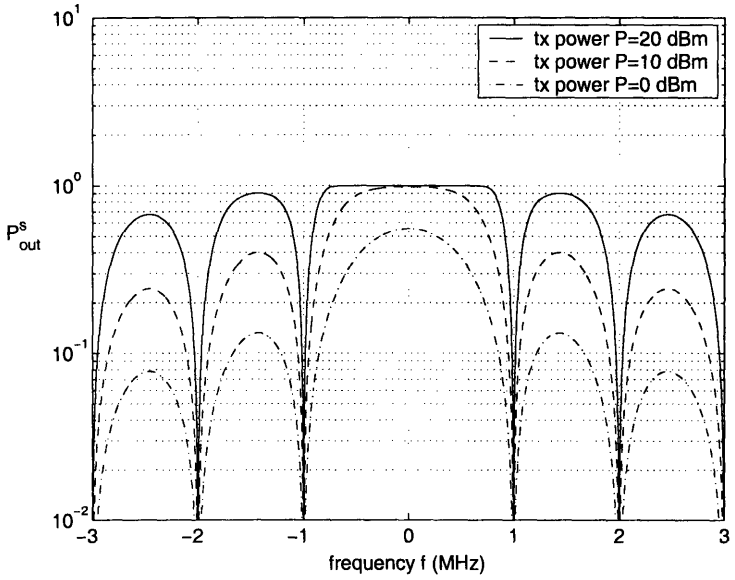

Figure 6.3: Spectral outage probability $P^{\mathrm{s}}_{\mathrm{out}}(f)$ versus frequency, for various transmitted powers P (square $p(t)$, $T = 10^{-6}\,\mathrm{s}$, $\lambda = 0.1\,\mathrm{m}^{-2}$, $b = 2$, $\sigma_{\mathrm{s}} = 10\,\mathrm{dB}$, $m(f) = -60\,\mathrm{dBm/Hz}$).

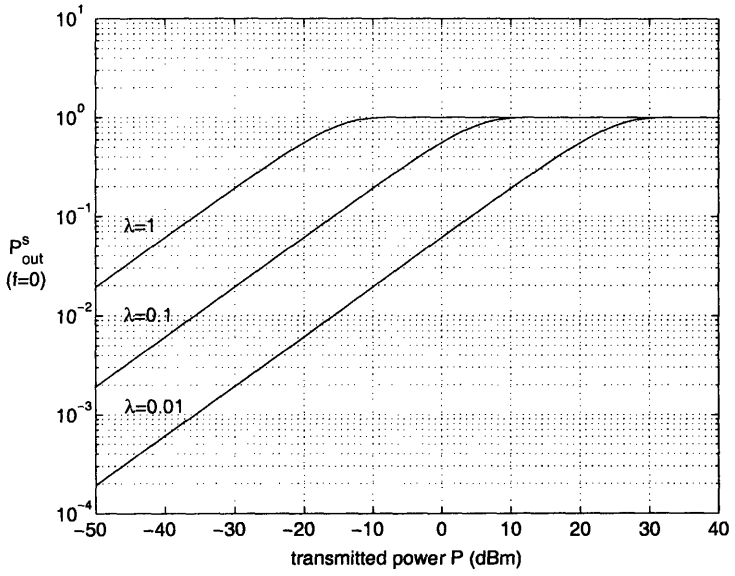

Figure 6.4: Spectral outage probability $P^{\mathrm{s}}_{\mathrm{out}}(f)$ evaluated at $f = 0$, for various interferer spatial densities λ in m^{-2} (square $p(t)$, $T = 10^{-6}\,\mathrm{s}$, $b = 2$, $\sigma_{\mathrm{s}} = 10\,\mathrm{dB}$, $m(f) = -60\,\mathrm{dBm/Hz}$).

Chapter 7

Conclusions and Future Research

This thesis investigates a mathematical model for communication subject to both interference and AWGN, where the spatial distribution of the nodes is captured by a Poisson field in the two-dimensional plane. We consider both the scenarios of *quasi-static* and *dynamic* nodes in a realistic wireless environment subject to path loss, log-normal shadowing, and fast Rayleigh fading. We then determine the statistical distribution of the cumulative interference at the output of a simple linear receiver, which leads directly to the characterization of the error probability and channel capacity.

We put forth the concept of *spectral outage probability* (SOP), which is can be used to quantify and limit the impact of the network interference on any receiver operating in the same frequency band. We determine the power spectral density (PSD) of the cumulative interference at any location in the plane, and then define and provide expressions for the corresponding SOP.

Finally, we quantify the cumulative interference distribution, error performance, channel capacity, PSD, and SOP as a function of various important system parameters, such as the signal-to-noise ratio, interference-to-noise ratio, amplitude loss exponent, and spatial density of the interferers. Our analysis clearly shows how the system performance depends on these parameters, thereby providing insights that may be of value to the network designer.

The proposed model is valid for any linear modulation scheme (e.g. M-PSK and M-QAM), and captures all the essential physical parameters that affect network in-

terference. Nevertheless, it is simple enough to allow a tractable analysis and provide fundamental insights. Finally, our work generalizes the conventional analysis of linear detection in the presence of AWGN and fast fading, allowing the traditional results to be extended to include the effect of interference.

Possible topics for future work include: 1) the extension of the proposed theory to both multi-antenna systems and ultrawideband systems; and 2) the application of the proposed theory to analyze the coexistence of ultrawideband and narrowband systems.

Appendix A

Derivation of the Interference Representation in (3.9)-(3.12)

In this appendix, we derive the complex baseband representation of the interference process $Y(t)$, as given in (3.9)-(3.12). The real passband signal $Y(t)$ can be projected onto the basis function $\psi_1(t) = \sqrt{\frac{2}{T}}\cos(2\pi f_c t)$ in the following way:

$$Y_1 = \int_0^T Y(t)\psi_1(t)dt \tag{A.1}$$

$$= \sum_{i=1}^{\infty} \int_0^T \left[\frac{\alpha_i e^{\sigma G_i}}{R_i^b} \sqrt{\frac{2E_i}{T}} \cos(2\pi f_c t + \theta_i + \phi_i) u(D_i - t) \right.$$

$$\left. + \frac{\alpha_i e^{\sigma G_i}}{R_i^b} \sqrt{\frac{2E_i'}{T}} \cos(2\pi f_c t + \theta_i' + \phi_i) u(t - D_i) \right] \sqrt{\frac{2}{T}} \cos(2\pi f_c t) dt \tag{A.2}$$

$$= \sum_{i=1}^{\infty} \frac{2}{T} \frac{\alpha_i e^{\sigma G_i}}{R_i^b} \left[\sqrt{E_i} \int_0^{D_i} \cos(2\pi f_c t + \theta_i + \phi_i) \cos(2\pi f_c t) dt \right.$$

$$\left. + \sqrt{E_i'} \int_{D_i}^T \cos(2\pi f_c t + \theta_i' + \phi_i) \cos(2\pi f_c t) dt \right] \tag{A.3}$$

$$= \sum_{i=1}^{\infty} \frac{2}{T} \frac{\alpha_i e^{\sigma G_i}}{R_i^b} \left[\frac{\sqrt{E_i}}{2} \int_0^{D_i} \cos(\theta_i + \phi_i) dt + \frac{\sqrt{E_i}}{2} \underbrace{\int_0^{D_i} \cos(4\pi f_c t + \theta_i + \phi_i) dt}_{\approx 0 \text{ if } f_c T \gg 1} \right.$$

$$+\frac{\sqrt{E_i'}}{2}\int_{D_i}^{T}\cos(\theta_i'+\phi_i)dt+\frac{\sqrt{E_i'}}{2}\underbrace{\int_{D_i}^{T}\cos(4\pi f_c t+\theta_i'+\phi_i)dt}_{\approx 0 \text{ if } f_cT\gg 1}\Bigg] \tag{A.4}$$

$$\approx\sum_{i=1}^{\infty}\frac{2}{T}\frac{\alpha_i e^{\sigma G_i}}{R_i^b}\left[\frac{\sqrt{E_i}}{2}\int_0^{D_i}\cos(\theta_i+\phi_i)dt+\frac{\sqrt{E_i'}}{2}\int_{D_i}^{T}\cos(\theta_i'+\phi_i)dt\right] \tag{A.5}$$

$$=\sum_{i=1}^{\infty}\frac{\frac{\alpha_i e^{\sigma G_i}}{T}\left[\sqrt{E_i}D_i\cos(\theta_i+\phi_i)+\sqrt{E_i'}(T-D_i)\cos(\theta_i'+\phi_i)\right]}{R_i^b} \tag{A.6}$$

$$=\sum_{i=1}^{\infty}\frac{e^{\sigma G_i}X_{i1}}{R_i^b}, \tag{A.7}$$

where

$$X_{i1}=\alpha_i\left[\sqrt{E_i}\frac{D_i}{T}\cos(\theta_i+\phi_i)+\sqrt{E_i'}\left(1-\frac{D_i}{T}\right)\cos(\theta_i'+\phi_i)\right].$$

To obtain (A.4), we used the relation $\cos(a)\cos(b)=\frac{1}{2}\cos(a+b)+\frac{1}{2}\cos(a-b)$. To obtain (A.5), we used the fact that both $\int_0^{D_i}\cos(4\pi f_c t+\theta_i+\phi_i)dt$ and $\int_{D_i}^{T}\cos(4\pi f_c t+\theta_i'+\phi_i)dt$ are close to zero with high probability, if $f_cT\gg 1$.

The signal $Y(t)$ can be projected onto the basis function $\psi_2(t)=\sqrt{\frac{2}{T}}\sin(2\pi f_c t)$ in an entirely analogous way, leading to

$$Y_2=\sum_{i=1}^{\infty}\frac{e^{\sigma G_i}X_{i2}}{R_i^b},$$

where

$$X_{i2}=\alpha_i\left[\sqrt{E_i}\frac{D_i}{T}\sin(\theta_i+\phi_i)+\sqrt{E_i'}\left(1-\frac{D_i}{T}\right)\sin(\theta_i'+\phi_i)\right].$$

Then, X_{i1} and X_{i2} can be combined in the complex r.v. $\mathbf{X}_i$ as

$$\begin{aligned}\mathbf{X}_i=&X_{i1}+jX_{j2}\\=&\alpha_i\left[\sqrt{E_i}\frac{D_i}{T}\cos(\theta_i+\phi_i)+\sqrt{E_i'}\left(1-\frac{D_i}{T}\right)\cos(\theta_i'+\phi_i)\right]\\&+j\alpha_i\left[\sqrt{E_i}\frac{D_i}{T}\sin(\theta_i+\phi_i)+\sqrt{E_i'}\left(1-\frac{D_i}{T}\right)\sin(\theta_i'+\phi_i)\right]\\=&\alpha_i\left[\sqrt{E_i}\frac{D_i}{T}e^{j(\theta_i+\phi_i)}+\sqrt{E_i'}\left(1-\frac{D_i}{T}\right)e^{j(\theta_i'+\phi_i)}\right]\end{aligned}$$

$$= \alpha_i e^{j\phi_i} \left[\frac{D_i}{T} \sqrt{E_i} e^{j\theta_i} + \left(1 - \frac{D_i}{T} \right) \sqrt{E_i'} e^{j\theta_i'} \right],$$

which completes the derivation.

Appendix B

Derivation of V_X in (3.16)

The expression for V_X given in (3.16) can be derived as follows, for $i \geq 1$:

$$\begin{aligned}
V_X =& \mathbb{V}\{X_{ij}\} \\
=& \mathbb{V}\left\{\frac{\alpha_i}{T}\left[\sqrt{E_i}D_i\cos(\theta_i+\phi_i)+\sqrt{E_i'}(T-D_i)\cos(\theta_i'+\phi_i)\right]\right\} \\
=& \overbrace{\frac{\mathbb{E}\{\alpha_i^2\}}{T^2}}^{=1}\Bigg[\mathbb{E}\{E_i\}\underbrace{\mathbb{E}\{D_i^2\}}_{=T^2/3}\underbrace{\mathbb{E}\{\cos^2(\theta_i+\phi_i)\}}_{=1/2} \\
&+\underbrace{\mathbb{E}\{2D_i(T-D_i)\}}_{=T^2/3}\mathbb{E}\{\sqrt{E_iE_i'}\cos(\theta_i+\phi_i)\cos(\theta_i'+\phi_i)\} \\
&+\mathbb{E}\{E_i'\}\underbrace{\mathbb{E}\{(T-D_i)^2\}}_{=T^2/3}\underbrace{\mathbb{E}\{\cos^2(\theta_i'+\phi_i)\}}_{=1/2}\Bigg] \\
=& \frac{\mathbb{E}\{E_i\}}{3}+\frac{1}{6}\left[\mathbb{E}\{\sqrt{E_iE_i'}\cos(\theta_i-\theta_i')\}+\mathbb{E}\{\sqrt{E_iE_i'}\}\underbrace{\mathbb{E}\{\cos(\theta_i+\theta_i'+2\phi_i)\}}_{=0}\right] \\
=& \frac{\mathbb{E}\{E_i\}}{3}+\frac{\mathbb{E}\{\sqrt{E_iE_i'}\cos(\theta_i-\theta_i')\}}{6}.
\end{aligned}$$

We have used the fact that $D_i \sim \mathcal{U}(0,T)$ and $\phi_i \sim \mathcal{U}(0,2\pi)$, and that the r.v.'s α_i, ϕ_i, D_i, $\sqrt{E_i}e^{j\theta_i}$, and $\sqrt{E_i'}e^{j\theta_i'}$ are mutually independent for a given i.[1] This completes the derivation.

[1]Note, however, that E_i and θ_i are *not* independent for a given i.

Appendix C

Derivation of the Distribution of Y in (3.17)

To derive the distribution of $\mathbf{Y}$ given in (3.17), we start with the following theorem.

Theorem C.1 (LePage Series Representation). *Let $\{\tau_i\}_{i=1}^{\infty}$ denote the arrival times of a one-dimensional Poisson process with rate λ; let $\{Z_i\}_{i=1}^{\infty}$ be a sequence of symmetric*[1] *i.i.d. r.v.'s, independent of the sequence $\{\tau_i\}$ and satisfying $\mathbb{E}|Z_i|^{\alpha} < \infty$. If $0 < \alpha < 2$, then*

$$\sum_{i=1}^{\infty} \frac{Z_i}{\tau_i^{1/\alpha}} \overset{\text{a.s.}}{\sim} \mathcal{S}\left(\alpha,\, \beta = 0,\, \gamma = \lambda C_{\alpha}^{-1} \mathbb{E}|W_i|^{\alpha}\right),$$

where

$$C_{\alpha} = \begin{cases} \frac{1-\alpha}{\Gamma(2-\alpha)\cos(\pi\alpha/2)}, & \alpha \neq 1, \\ \frac{2}{\pi}, & \alpha = 1. \end{cases}$$

Proof. See [8]. For an alternative proof based on the influence function method, see [3, 11]. □

If an homogeneous Poisson point process *in the plane* has rate λ, and R_i denotes the distance of node i to the origin, then the sequence $\{R_i^2\}_{i=1}^{\infty}$ represents Poisson arrival times *on the line* with the constant arrival rate $\lambda\pi$. This can be easily shown by mapping the Poisson point process from Cartesian into polar coordinates, and then applying the

[1] *A r.v. X is said to be symmetric if X and $-X$ have the same p.d.f.*

mapping theorem [12]. Using this fact, we can then apply the above theorem to (3.5) and write

$$Y_1 = \sum_{i=1}^{\infty} \frac{e^{\sigma G_i} X_{i1}}{R_i^b} = \sum_{i=1}^{\infty} \frac{\overbrace{e^{\sigma G_i} X_{i1}}^{\text{symmetric}}}{\underbrace{(R_i^2)^{b/2}}_{\tau_i}} \overset{\text{a.s.}}{\sim} \mathcal{S}\left(\alpha = \frac{2}{b},\, \beta = 0,\, \gamma = \lambda \pi C_{2/b}^{-1} \mathbb{E}|e^{\sigma G_i} X_{i1}|^{2/b}\right), \tag{C.1}$$

where $0 < \alpha < 2$ (or equivalently, $b > 1$). Note that X_{i1}, whose expression is given in (3.7), is symmetric due to the uniform phase ϕ_i. As a result, $e^{\sigma G_i} X_{i1}$ is also symmetric. Using the moment property of log-normal r.v.'s, i.e., $\mathbb{E}\{e^{kG}\} = e^{k^2/2}$ with $G \sim \mathcal{N}(0,1)$, (C.1) simplifies to

$$Y_1 \overset{\text{a.s.}}{\sim} \mathcal{S}\left(\alpha = \frac{2}{b},\, \beta = 0,\, \gamma = \lambda \pi C_{2/b}^{-1} e^{2\sigma^2/b^2} \mathbb{E}|X_{i1}|^{2/b}\right).$$

In an entirely analogous way, we can show that

$$Y_2 \overset{\text{a.s.}}{\sim} \mathcal{S}\left(\alpha = \frac{2}{b},\, \beta = 0,\, \gamma = \lambda \pi C_{2/b}^{-1} e^{2\sigma^2/b^2} \mathbb{E}|X_{i2}|^{2/b}\right),$$

and thus write the distribution of $\mathbf{Y} = Y_1 + jY_2$ as

$$\mathbf{Y} \overset{\text{a.s.}}{\sim} \mathcal{S}_c\left(\alpha = \frac{2}{b},\, \beta = 0,\, \gamma = \lambda \pi C_{2/b}^{-1} e^{2\sigma^2/b^2} \mathbb{E}|X_{ij}|^{2/b}\right),$$

where $b > 1$. This is the result in (3.17), and the derivation is complete.

Appendix D

Derivation of the Distribution of A in (3.20)

To derive the distribution of A given in (3.20), we start with the following theorem.

Theorem D.1. *Let $\{\tau_i\}_{i=1}^{\infty}$ denote the arrival times of a one-dimensional Poisson process with rate λ; let $\{W_i\}_{i=1}^{\infty}$ be a sequence of nonnegative i.i.d. r.v.'s, independent of the sequence $\{\tau_i\}$ and satisfying $\mathbb{E}|W_i|^{\alpha} < \infty$. If $0 < \alpha < 1$, then*

$$\sum_{i=1}^{\infty} \frac{W_i}{\tau_i^{1/\alpha}} \overset{\text{a.s.}}{\sim} \mathcal{S}\left(\alpha,\, \beta = 1,\, \gamma = \lambda C_{\alpha}^{-1} \mathbb{E}|W_i|^{\alpha}\right),$$

where

$$C_{\alpha} = \begin{cases} \frac{1-\alpha}{\Gamma(2-\alpha)\cos(\pi\alpha/2)}, & \alpha \neq 1, \\ \frac{2}{\pi}, & \alpha = 1. \end{cases}$$

Proof. See [8]. □

Using the Poisson mapping theorem as in Appendix C (i.e., the sequence $\{R_i^2\}_{i=1}^{\infty}$ represents Poisson arrival times on the line with arrival rate $\lambda\pi$), we can then apply

the above theorem to (3.15) and write

$$A = \sum_{i=1}^{\infty} \frac{e^{2\sigma G_i}}{R_i^{2b}} = \sum_{i=1}^{\infty} \frac{\overbrace{e^{2\sigma G_i}}^{W_i}}{\underbrace{(R_i^2)^b}_{\tau_i}} \overset{\text{a.s.}}{\sim} \mathcal{S}\left(\alpha = \frac{1}{b},\, \beta = 1,\, \gamma = \lambda \pi C_{1/b}^{-1} \mathbb{E}|e^{2\sigma G_i}|^{1/b}\right), \quad \text{(D.1)}$$

where $0 < \alpha < 1$ (or equivalently, $b > 1$). Using the moment property of log-normal r.v.'s, i.e., $\mathbb{E}\{e^{kG}\} = e^{k^2/2}$ for $G \sim \mathcal{N}(0,1)$, (D.1) simplifies to

$$A \overset{\text{a.s.}}{\sim} \mathcal{S}\left(\alpha = \frac{1}{b},\, \beta = 1,\, \gamma = \lambda \pi C_{1/b}^{-1} e^{2\sigma^2/b^2}\right),$$

where $b > 1$. This is the result in (3.20), and the derivation is complete.

Bibliography

[1] A. J. Viterbi and I. M. Jacobs, "Advances in coding and modulation for noncoherent channels affected by fading, partial band, and multiple-access interference," in *Advances in Communication Systems: Theory and Applications*, vol. 4. New York: Academic Press Inc., 1975, pp. 279–308.

[2] N. Beaulieu and A. Abu-Dayya, "Bandwidth efficient QPSK in cochannel interference and fading," *IEEE Trans. Commun.*, vol. 43, no. 9, pp. 2464–2474, 1995.

[3] E. Sousa, "Performance of a spread spectrum packet radio network link in a Poisson field of interferers," *IEEE Trans. Inform. Theory*, vol. 38, no. 6, pp. 1743–1754, 1992.

[4] J. Ilow, D. Hatzinakos, and A. Venetsanopoulos, "Performance of FH SS radio networks with interference modeled as a mixture of gaussian and alpha-stable noise," *IEEE Trans. Commun.*, vol. 46, no. 4, pp. 509–520, 1998.

[5] X. Yang and A. Petropulu, "Co-channel interference modeling and analysis in a Poisson field of interferers in wireless communications," *IEEE Trans. Signal Processing*, vol. 51, no. 1, pp. 64–76, 2003.

[6] S. Govindasamy, F. Antic, D. Bliss, and D. Staelin, "The performance of linear multiple-antenna receivers with interferers distributed on a plane," in *Proc. IEEE Workshop on Signal Proc. Advances in Wireless Commun.*, 2005, pp. 880–884.

[7] M. Weisenhorn and W. Hirt, "Uncoordinated rate-division multiple-access scheme for pulsed UWB signals," *IEEE Trans. Veh. Technol.*, vol. 54, no. 5, pp. 1646–1662, 2005.

[8] G. Samoradnitsky and M. Taqqu, *Stable Non-Gaussian Random Processes.* Chapman and Hall, 1994.

[9] W. Feller, *An Introduction to Probability Theory and Its Applications.* Wiley, 1971, vol. 2.

[10] C. L. Nikias and M. Shao, *Signal Processing with Alpha-Stable Distributions and Applications.* Wiley-Interscience, 1995.

[11] V. M. Zolotarev, *One-Dimensional Stable Distributions.* American Mathematical Society, 1986.

[12] J. Kingman, *Poisson Processes.* Oxford University Press, 1993.

[13] A. Goldsmith, *Wireless Communications.* Cambridge University Press, 2005.

[14] J. Andersen, T. Rappaport, and S. Yoshida, "Propagation measurements and models for wireless communications channels," *IEEE Commun. Mag.*, vol. 33, no. 1, pp. 42–49, 1995.

[15] J.-P. Linnartz, *Narrowband Land-Mobile Radio Networks.* Artech House Publishers, 1993.

[16] G. L. Stüber, *Principles of Mobile Communication.* Springer, 2000.

[17] O. Andrisano, V. Tralli, and R. Verdone, "Millimeter waves for short-range multimedia communication systems," *Proc. IEEE*, vol. 86, no. 7, pp. 1383–1401, 1998.

[18] A. Giorgetti and M. Chiani, "Influence of fading on the gaussian approximation for BPSK and QPSK with asynchronous cochannel interference," *IEEE Trans. Wireless Commun.*, vol. 4, no. 2, pp. 384–389, 2005.

[19] J. Proakis, *Digital Communications.* McGraw-Hill, 2000.

[20] M. Z. Win and J. H. Winters, "Virtual branch analysis of symbol error probability for hybrid selection/maximal-ratio combining in Rayleigh fading," *IEEE Trans. Commun.*, vol. 49, no. 11, pp. 1926–1934, Nov. 2001.

[21] M. K. Simon and M.-S. Alouini, *Digital Communication over Fading Channels.* Wiley-IEEE Press, 2004.

[22] J. Craig, "A new, simple and exact result for calculating the probability of error for two-dimensional signal constellations," in *Proc. IEEE Military Commun. Conf.*, 1991, pp. 571–575.

[23] J. Chambers, C. Mallows, and B. Stuck, "A method for simulating stable random variables," *J. Amer. Statist. Assoc.*, vol. 71, pp. 340–344, 1976.

[24] T. M. Cover and J. A. Thomas, *Elements of Information Theory.* Wiley-Interscience, 1991.

[25] D. Tse and P. Viswanath, *Fundamentals of Wireless Communication.* Cambridge University Press, 2005.

[26] M. Abramowitz and I. A. Stegun, *Handbook of Mathematical Functions.* Dover Publications, 1965.

[27] A. Papoulis and S. U. Pillai, *Probability, Random Variables and Stochastic Processes.* McGraw-Hill, 2001.

[28] M. K. Simon, S. M. Hinedi, and W. C. Lindsey, *Digital Communication Techniques: Signal Design and Detection.* Prentice Hall, 1994.

[29] M. Z. Win, "A unified spectral analysis of generalized time-hopping spread-spectrum signals in the presence of timing jitter," *IEEE J. Select. Areas Commun.*, vol. 20, no. 9, pp. 1664–1676, Dec. 2002.